Shear Localization in Dynamic Deformation: Microstructural Evolution

YONGBO XU, JINGHUA ZHANG, YILONG BAI, and MARC ANDRÉ MEYERS

Investigations made by the authors and collaborators into the microstructural aspects of adiabatic shear localization are critically reviewed. The materials analyzed are low-carbon steels, 304 stainless steel, monocrystalline Fe-Ni-Cr, Ti and its alloys, Al-Li alloys, Zircaloy, copper, and Al/SiC_p composites. The principal findings are the following: (a) there is a strain-rate-dependent critical strain for the development of shear bands; (b) deformed bands and white-etching bands correspond to different stages of deformation; (c) different slip activities occur in different stages of band development; (d) grain refinement and amorphization occur in shear bands; (e) loss of stress-carrying capability is more closely associated with microdefects rather than with localization of strain; (f) both crystalline rotation and slip play important roles; and (g) band development and band structures are material dependent. Additionally, avenues for new research directions are suggested.

DOI: 10.1007/s11661-007-9431-z

I. INTRODUCTION

LOCALIZED shear deformation in the form of intensive deformation in a narrow band generated during dynamic deformation under high strain rates has been a topic of great interest for decades and, thus, a great deal of investigation has been conducted experimentally and theoretically since Zener and Hollomon's classic article of 1944.[1] It is interesting to note that Tresca[2] had already observed this phenomenon in the nineteenth century. Localized shear is an important mode of deformation; it leads to catastrophic failure with low ductility and it occurs frequently during high-strain-rate deformation, such as is found in ballistic impact, explosive fragmentation, high-speed shaping and forming, dynamic compaction and welding, machining, and grinding. This deformation mode may also occur during quasi-static loading, such as uniaxial extension and cyclic fatigue. The failure of metallic glasses and, in particular, bulk metallic glasses is a classic example of shear localization, and it has been shown by Lewandowski and Greer[3] that temperature plays a role: significant temperature rises were measured. Similarly, nanocrystalline metals are prone to shear localization when deformed at low strain rates and, although the imposed displacement velocities are small, the evolution of shear bands is dynamic and leads to early failure by virtue of a near absence of work hardening (*e.g.*, Jia *et al.*[4] and Wei *et al.*[5]). The phenomenon is clearly recognizable in most steels and in other metals, including aluminum alloys, copper, titanium, zirconium, and uranium and their alloys; aluminum composites reinforced with SiC particles and whiskers; and engineering plastics.

Mechanical engineers have focused their efforts on the macrodescription of the constitutive model, developing the criteria required for the plastic deformation instability (Recht in 1964,[6] Culver in 1973,[7] Clifton in 1980,[8] Bai in 1981,[9] Burns and Trucano in 1982,[10] Pan in 1983,[11] Semiatin *et al.* in 1984,[12] Wu and Freund in 1984,[13] Wright and Batra in 1985,[14] Fressengeas and Molinari in 1987,[15] Johnson in 1981,[16] Drew and Flaherty in 1984,[17] Lemonds and Needleman in 1986,[18] Tvergaard in 1987,[19] and Anderson *et al.* in 1990[20]). Most of the approaches consist of a combination of mechanical and thermal instability analysis. On the other hand, materials scientists have focused on the material and structural aspects of localized shear deformation, emphasizing the effect of the microstructures on the formation of the shear bands.

Regarding the microstructural aspects of shear localization, there are a number of reviews: Rogers,[21,22] Stelly and Dormeval,[23] Timothy,[24] Murr,[25] Dormeval,[26] and Meyers.[27,28] Among the numerous articles on the topic, the articles indicated in Table I are noteworthy.

In this article, we will review results of the microstructural aspects of the adiabatic shear localization generated under an imposed strain rate range of 10^3 to 10^4 s^{-1} at ambient temperature, resulting from research carried out by the authors over the past 20 years.

YONGBO XU and JINGHUA ZHANG, Professors, are with the Shenyang National Laboratory of Materials Sciences, Institute of Metal Research, Chinese Academy of Sciences, Shenyang 110016, P.R. China. Contact e-mail: ybxu@imr.ac.cn YILONG BAI, Professor, is with the State Key Laboratory for Non-Linear Mechanics of Continuous Media, Institute of Mechanics, Chinese Academy of Sciences, Beijing, P.R. China. MARC ANDRE′ MEYERS, Professor, is with the Materials Science and Engineering Program and Department of Mechanical and Aerospace Engineering, University of California at San Diego, La Jolla, CA 92093-0411.

This article is based on a presentation made in the symposium entitled "Dynamic Behavior of Materials," which occurred during the TMS Annual Meeting and Exhibition, February 25–March 1, 2007 in Orlando, Florida, under the auspices of The Minerals, Metals and Materials Society, TMS Structural Materials Division, and TMS/ASM Mechanical Behavior of Materials Committee.

Article published onlined February 13, 2008

Table I. Principal Research Articles on Adiabatic Shear Bands

Ti and alloys	Grebe *et al.*[29]	Stelly *et al.*[30]
	Marchand and Duffy[31]	Shockey *et al.*[32]
	Me-Bar and Shechtman[33]	Timothy and Hutchings[34]
	Meyers *et al.*[35,36]	da Silva and Ramesh[37]
	Chichili *et al.*[38]	Xue *et al.*[39]
Steels	Hartley *et al.*[40]	Bai *et al.*[41,42]
	Chen *et al.*[43]	Xu *et al.*[44]
	Manion and Stock[45]	Glenn and Leslie[46]
	Thornton and Heiser[47]	Wingrove[48]
	Manion and Wingrove[49]	Woodward and Aghan[50]
	Derep[51]	Stelly *et al.*[52]
	Wright and Batra[53]	Giovanola[54]
	Cho *et al.*[55]	Liao and Duffy[56]
	Beatty *et al.*[57]	Meunier *et al.*[58]
	Wittman *et al.*[59,60]	Lins *et al.*[180]
Stainless steels	Xue *et al.*[61,62]	Meyers *et al.*[63]
	Batra and Zhang[64]	Lee *et al.*[65]
	Cerreta *et al.*[67]	Xue and Gray[66]
Zirconium	Kad *et al.*[68]	——
Aluminum alloys	Bai *et al.*[69]	Chen and Vecchio[70]
Uranium, hafnium	Magness[71]	Subhash *et al.*[72]
Tantalum	Chen *et al.*[43]	Vecchio *et al.*[74]
	Nemat Nasser *et al.*[75]	Hynes and Vecchio[193]

The emphasis is placed on the conditions of band formation, microstructural characterization, and microstructural evolution.

II. EXPERIMENTAL METHODS

A. *Dynamic Tests*

The localized shear bands were generated by three methods, as shown in Figure 1.

(a) The thin-walled tube with integral circular flanges matching the torsional impedance of the aluminum bar for dynamic torsional and impact tests, which were performed by split Hopkinson torsion bar (SHTB) (Figure 1(a)).
(b) The hat-shaped specimen method (Figure 1(b)), which was developed by Meyers and Manwaring[76] and has been successfully used to generate a shear localization region in a number of metals, of Ti,[36] steels,[57] Al alloys,[77] Ta,[43] Zircaloy,[68] and stainless steel.[61,62,66,67] It should be noted that this is a "forced" shear localization process, in contrast to other experimental techniques, which allow the bands to form naturally. Detailed finite element method (FEM) computations have been carried out on this geometry by Los Alamos National Laboratory (LANL) researchers.[78,79]
(c) The explosive collapse of a thick-walled cylinder (TWC) under controlled and prescribed conditions (Figure 1(c)), which was developed by Nesterenko and Bondar[80] and applied to Ti,[81] stainless steel,[62] and tantalum.[43] Detailed calculations are reported by Xue *et al.*[82]

B. *SHTB Modification*

There is a difficulty associated with application of the usual SHTB for the study of the microstructure evolution process during shear localization, because of the transient nature of the process and the localizing field. Therefore, Xue *et al.*[83] modified the usual SHTB by attaching an unloading bar and an inside-pushed connector. This modification eliminates the effect of loading reverberation on postmortem observations, making the combined measurements of the mechanical parameters (stress and strain) and the relevant transient microstructural observation possible.

C. *Microstructural Characterization*

The small width of the bands (on the order of 1 to 500 μm) renders microscopic examination difficult. In particular, it is very hard to prepare the thin-foil specimens for transmission electron microscopy (TEM) examination, because the perforation produced using ordinary methods such as double-jet polishing and ion milling generally does not coincide with the shear-band area. Two preparation methods are noteworthy.

(a) The "cross section and butt" method, used to make the thin foils for TEM observations in some cases.[84] The specimens are mechanically ground and dimpled to a thickness of less than 20 μm. Finally, the ion-beam milling is carried out with Ar^+ bombardment at 4 KV and a grazing incidence angle of 10 deg.
(b) Electropolishing followed by ion milling: The method described by Wittman *et al.*[60] and Kad *et al.*[68] was also used, in which the perforation produced by electropolishing is gradually enlarged until it intersects the band. Figure 2(a) shows the perforation before and after it intersects the shear band. In this manner, one can, after viewing the band and hole by optical microscopy, ensure that TEM is focused on the appropriate region. Figure 2(b) shows a Zircaloy specimen with the perforation intersecting a band.

There are more modern sample preparation techniques, such as focused ion beam, that it is hoped will shed some additional light on the band structure. The microstructure and its evolution process were characterized by scanning electron microscopy (SEM), confocal laser scanning microscopy (CFLSM), field emission scanning electron microscopy (FESEM), TEM, and high-resolution electron microscopy (HREM).

III. RESULTS AND DISCUSSION

A. *Evolution Process of the Shear Band*

The processes of formation and evolution of the shear bands have stimulated a considerable number of

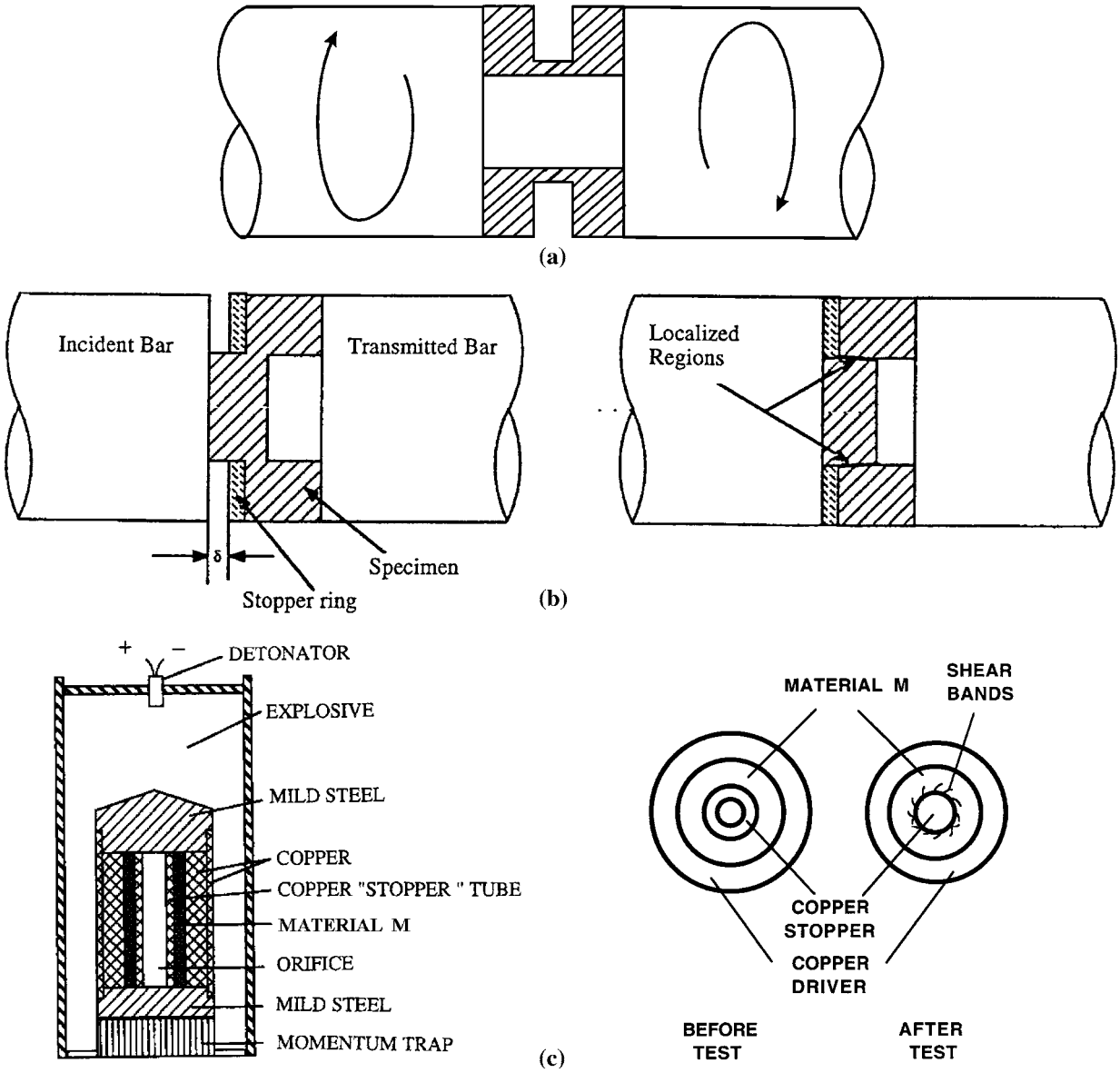

Fig. 1—Experimental methods used to generate the shear bands: (*a*) thin-walled-tube specimen for torsion loading, (*b*) hat-shaped specimen for forced shear localization, and (*c*) TWC technique using explosive collapse.

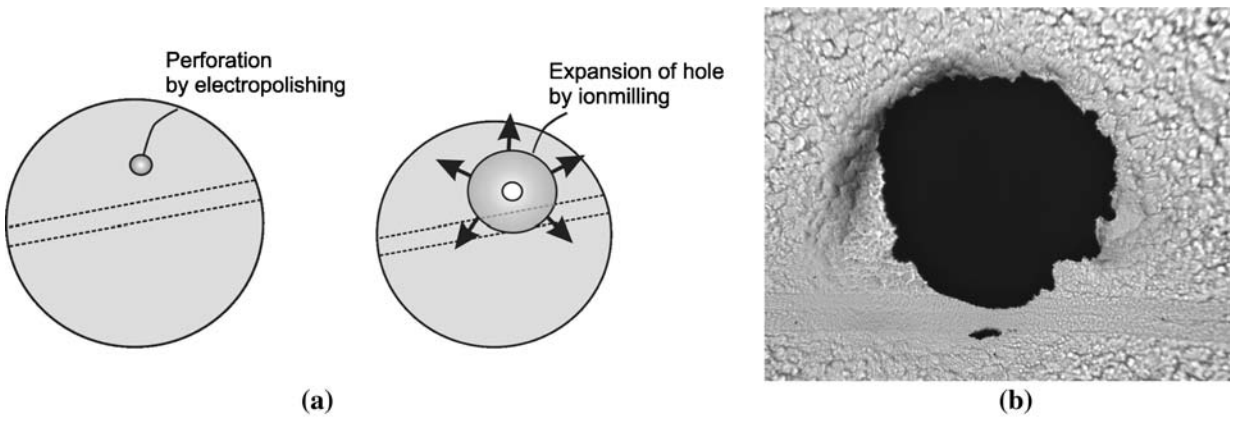

Fig. 2—(*a*) Sequential electropolishing ion-milling technique and (*b*) shear band in Zircaloy at edge of perforation (courtesy of B. Kad).

theoretical and experimental investigations. Among the analytical approaches, the following are noteworthy:

(a) criteria proposed by Zener and Hollomon,[1] Recht,[6] and Culver,[7] based exclusively on the effects of work hardening, thermal softening, and strain rate sensitivity;
(b) perturbation analyses of Molinari and Clifton,[85] Clifton,[8] Bai,[9] and Grady and Kipp,[86] which represent a significant advance over the simpler first-generation analyses;
(c) finite element formulation in various forms (*e.g.*, Kuriyama and Meyers[87]); and
(d) spacing of shear bands, which was theoretically treated by Grady and Kipp,[86] Ockendon and Wright,[88] and Molinari.[89]

Additional noteworthy studies are the ones by Clifton *et al.* in 1984,[90] Bai *et al.* in 1986,[91] Wright and Batra in 1987,[92] Shawki and Clifton in 1989,[93] Xing *et al.* in 1991,[94] and Liao and Duffy in 1998.[95] A number of scaling laws have been obtained (Backman *et al.* in 1986,[96] Bai in 1989,[97] Dodd and Bai in 1987,[98] and Anand *et al.* in 1990[99]). However, the analysis of localized plastic shear deformation is still currently limited by a lack of critical comparisons of theory and experiment. Some experimental attempts to measure the process of shear localization have been made. Costin *et al.* in 1979[100] are known to be the first to measure the temperature history of shear localization; later Hartley *et al.* in 1987[101] and Marchand and Duffy in 1988[102] have improved their infrared technique and measured the temperature distribution and history. They assumed that the localized shear process was divided into three consecutive stages. In the first stage, the grid lines incline but remain straight, implying that the deformation is homogeneous. In the second stage, the grid lines become slightly curved, indicating inhomogeneous deformation. In the third and final stage, the grid lines appear discontinuous, indicating shear-band formation. Marchand and Duffy[102] and Giovanola in 1988[103] have independently observed the transient deformation field of the localized shear process by means of high-speed photography and a grid pattern. More recently, Guduru *et al.*[141] obtained detailed *in-situ* temperature profiles at the shear-band tips in a C 300 maraging steel. They focused on the tip of the band with a two-dimensional infrared radiation (IR) array with an acquisition rate of 10^6 frames per second. Each detector was 100×100 μm. They observed that the front contained "hot spots" with a spacing of ~0.25 to 1 mm, which they attributed to vorticity. They report local temperature rises of up to 600 K. Some vortex-like features are shown later (Figure 12).

All these works certainly have blazed a trail in the experimental study of the localized shear process, but they have not revealed the evolution process of the microstructure occurring during shearing and have not clarified the relationship of the mechanical parameters with the corresponding microstructures in the bands. The main reason for this is that the original SHTB could not be used to study the microstructure evolution occurring during shear localization. Xue *et al.*[83] modified the original SHTB by a series of interrupted tests, which enabled them to combine ingeniously the measurements of the mechanical parameters (stress and strain) at successive points on the stress-strain curve with correlated microstructure observation, and to follow the formation and evolution processes of the shear band. Figure 3 shows four interrupted tests on the four stress-strain curves with four prescribed loading durations, labeled T9-38, T9-39, T9-37, and T9-21, for Ti-6Al-4V alloys subjected to dynamic torsional loading at average strain rates of about 3.1×10^3 s^{-1}.[42] There is a node in the stress-strain curve at which the average critical strain is about 0.166. The T9-38 at point 1 is loaded for 450 μs, close to the critical time, showing a maximum strain of 0.160, and it represents the state near the critical point. Within the curve, there are no kinks, implying that the specimen is still in homogeneous deformation, and no microstructure change is observed during this regime of homogeneity. Beyond this point, the stress drops slowly. The T9-39 at point 2, loaded for about 550 μs, attained a nominal strain of 0.196 before unloading. Local maxima and minima in the stress-strain curve for this sample is suggestive of inhomogeneous deformation. Metallographic observation displays the distinct occurrence of shear localization; the width of the local shear zone is about 44 μm and the maximum shear strain is 1.07, five times the average value. A tiny elliptical void can be seen within the shear zone. Of even more interest is that the width of the local shear zone is much narrower than the size of the grain, but its extension covers several grains. Loaded for 650 μs, the T9-37 at point 3 gained a nominal strain of 0.219. Severe localized shear band appeared. Figure 4 exhibits a drastic change in the microstructure in the localized shear zone. Obviously, microvoids have grown and some of them coalesced into a large crack, as shown in Figure 5; they even extended from one grain to another. There are still some uncracked segments in the shear band. The width of the shear band and the localized strain are uneven along the shear band. Near the crack tip, the shear band is 20 μm wide, attaining a strain of 2.14; apart from the crack zone, on the other

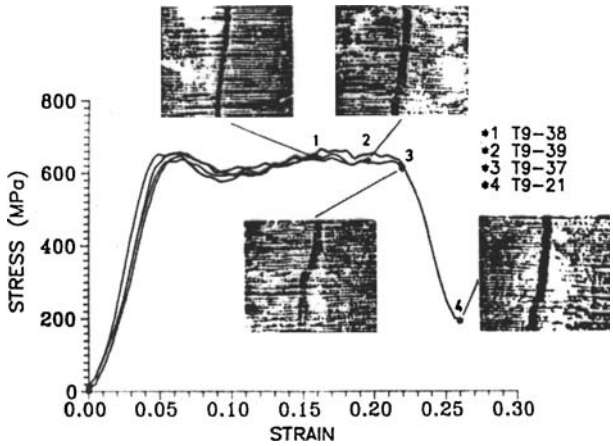

Fig. 3—Stress-strain response of Ti-6Al-4V alloys subjected to dynamic torsional loading and the corresponding patterns of the inside scribe lines.

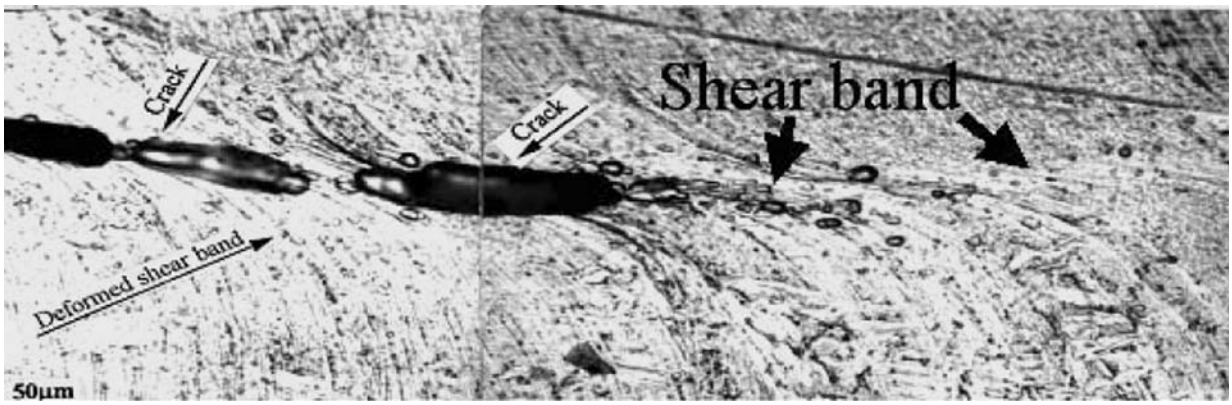

Fig. 4—Microvoids in the shear band generated during dynamic torsional loading in Ti-6Al-4V alloy.

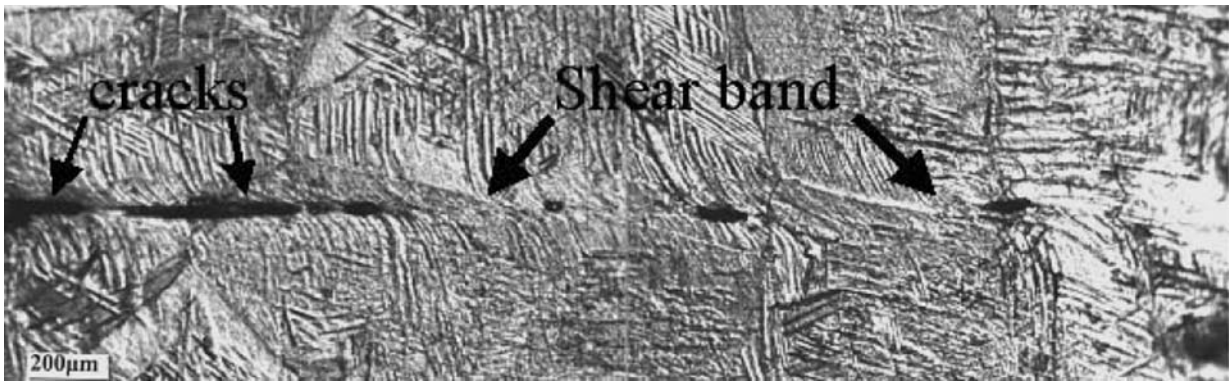

Fig. 5—Shear band transversing several grains and coalescence of microcracks along the shear band during localization in Ti-6Al-4V alloy.

hand, it has a strain of 1.07 and width of about 60 μm. The occurrence of the shear band does not significantly affect the capacity of the material for continued deformation (point 3 in Figure 3). In fact, the steep drop in the shear stress appears only after point 3. The specimen T9-21 at point 4, with a loading duration of 750 μs, presents a greater average strain of 0.26 but much lower stress, only one-third of that at the critical point. Figure 5 displays the morphology of the critical zone. A long straight crack has formed along the shear band. The half-width of the band is about 10 μm. Typically, the sudden drop in the stress-strain curve is described as catastrophic failure, due to the localized shearing.[31] These observations of both stress-strain response behavior and related microstructure suggest that the critical mechanism governing the loss in load-bearing capacity is the microcrack coalescence within the band, rather than the shear-band formation. However, the possibility that the cracks were generated after deformation cannot be excluded.

Similarly, Figure 6 shows the localized process of shear deformation in low-carbon steels subjected to a dynamic torsion.[44] The experiment reveals that when the average strain is approximately 0.34, corresponding to the loading duration of 550 μs (not shown in Figure 6), the fiducial line on the sample shows homogeneous deformation, and there is no shear localization to be found on the cross section of the specimen, which implies that the specimen tested is still in the work-hardening stage. However, as the shear strain increases to about 0.36, corresponding to the loading time of 750 μs (Figure 6(a)), shear localization occurs. After this point, the specimen appears to work soften with increasing shear stress. When the loading time is about 890 μs, the shear deformation appears to be apparent and very narrow bands are formed, as shown in Figure 6(c). The widths of the bands for the three times (750, 850, and 890 μs) are 310, 110, and 100 μm, respectively, which implies that the localized deformation is a progressive process during which shear deformation becomes gradually localized. The widths are marked in Figure 6. The longer the loading time, the narrower the band.

One more example is given clearly in Figure 7, showing a series of interrupted tests performed on an Al-Li alloy with the modified Split Hopkinson pressure bar (SHPB) at an average strain rate of about 2.3×10^3 s^{-1}.[77] It was found that, when the average strain is approximately 0.10, corresponding to a loading time of 40 μs, the deformation appears to be homogeneous, and there is no shear localization to be recognized on the cross section of the specimen, as shown in Figure 7(a). This implies that the specimen tested is still in work hardening. However, as the average strain

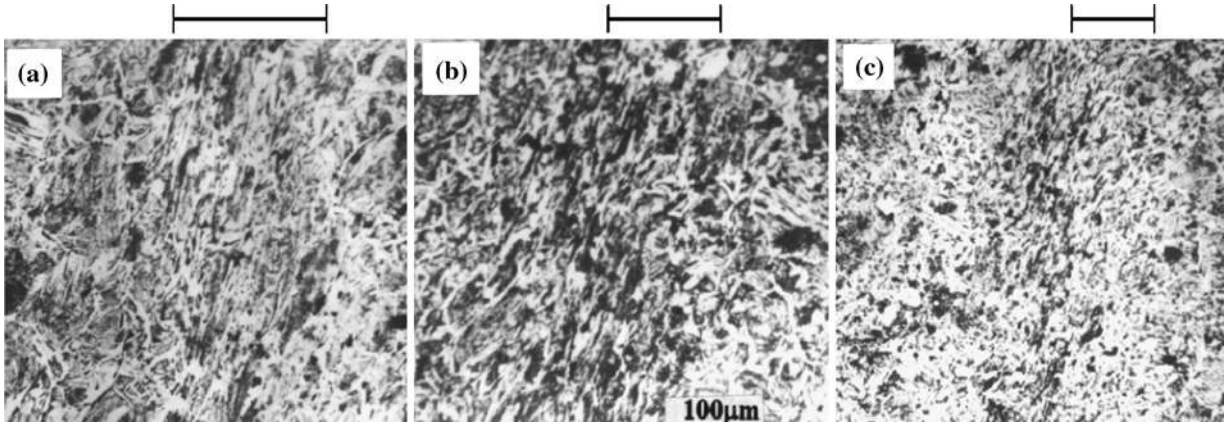

Fig. 6—Developed process of shear localization corresponding to different loading times of (*a*) 750, (*b*) 850, and (*c*) 890 μs.

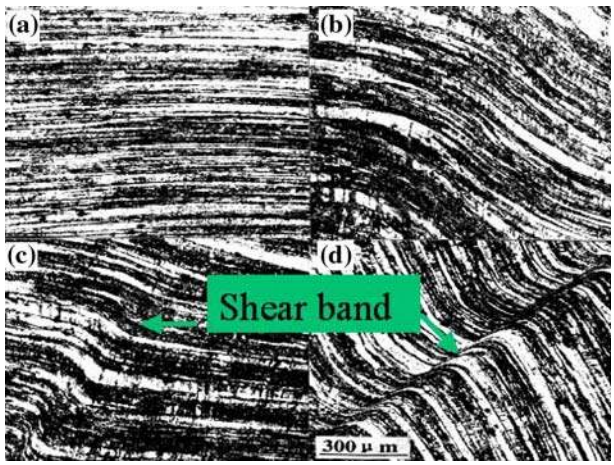

Fig. 7—Evolution of localized shear as strain is increased in Al-Li alloy subjected to dynamic impact compression: (*a*) loading time 40 μs, average strain 0.1; (*b*) loading time 100 μs, average strain 0.22, and local strain 3; (*c*): loading time 120 μs, average strain 0.28, and local strain 0.8.

increases from 0.10 to 0.17, corresponding to a loading time of 80 μs, localized shear deformation with a local strain of 0.75 starts to occur, as shown in Figure 7(b). Beyond this point, the specimen appears to work soften as the loading time increases; localized deformation becomes more apparent, as shown in Figure 7(c). When loading time is about 120 μs, the shear band narrows, with a width of 25 μm and local strain of 0.8, as shown in Figure 7(d). Thus, the evolution of localized deformation is a rapid, progressive process during which the localization becomes more apparent and the width of the band becomes gradually narrower. This can be rationalized in terms of the Bai–Dodd and Grady equations that predict the shear-band thickness; they will be presented in Section H.

B. *Conditions for the Occurrence of the Shear Band*

The criterion for shear-band formation has been one of the most interesting research challenges; for over two decades, approaches have been focused on the theoretical treatments, consisting of a combination of mechanical instability analysis with thermal model. These analyses generally concur that, once the critical strain corresponding to the macroscopic maximum in load on a stress-strain curve of the material has been achieved, the shear bands form (Culver,[7] Dormeval in 1981,[104] Burns and Trucano in 1982,[10] Bai in 1987,[105] Olson *et al*. in 1981,[106] Staker in 1981,[107] Semiatin and Lahoti in 1983,[108] Wu and Freund in 1987,[109] Clifton and Duffy,[90] Backman and Finnegan in 1973,[110] Bedford and Wingrove in 1974[111]). Based on the thermoplastic instability in simple shearing, Bai,[9] Clifton,[8] and Timothy and Hutchings[112] carried out linear perturbation analyses and suggested a maximum load required for the shear-band formation; this is in agreement with the maximum shear stress criterion proposed by Culver.[7] Molinari[113] provided a more advanced, nonlinearized perturbation analysis. Wright[114] extended this treatment and proposed a double instability/localization criterion. They were able to separate the two events. Staker[107] examined the effect of the AISI 4340 steel tempering temperature on the susceptibility to ''transformed'' band formation. He proposed that there exists a critical strain for the formation of transformed shear bands that depends on the heat treatment condition of the steel. Taking into account thermal softening and conduction, Recht[6] proposed a critical strain rate as a criterion for the occurrence of the shear band. In fact, the analysis made by Clifton[8] arrives at the same expression as that derived by Recht for high-speed machining. It should be pointed out that all analyses mentioned here lack sufficient supporting experimental data. Rogers pointed out in his review[22] that ''the above results also bear on the problem of whether or not a 'critical strain rate' exists for adiabatic shearing in a given material. The above results and others obtained at Drexel appear to support this concept; the results of Timothy and Hutchings do not.'' Rogers pointed out again that ''large strain can be achieved quasi-statically in steel without transformed band formation; hence, provided that a minimum strain achieved, there must exist a strain rate above which the removal of heat from the region of deformation is sufficiently limited that the temperature can rise above that needed for transformation to

occur—a critical strain rate." Zurek in 1994[115] studied the white-etching bands in 4340 steel and found that the average strain of 0.5 and the associated average strain rate of 1.8×10^4 s^{-1} were sufficient to induce an adiabatic shear instability in this steel, implying that both strain and strain rate should be required for the white-etching band formation. Bai in 1982[116] predicted in his analysis that the condition for the band formation should include both the stress and the strain rate.

Bai's prediction[116] is verified by the experimental investigations of the aluminum and titanium alloys.[77,117] Figure 8 shows two types of shear bands formed in a titanium alloy subjected to dynamic impact compression. It reveals that as the strain rate increases, localized shear deformation develops gradually, and when the strain rate reaches 1.75×10^3 s^{-1}, the deformed shear bands appear first as shown in Figure 8(a); as deformation proceeds, the width of the band becomes gradually narrower. When the strain rate is approximately 2×10^3 s^{-1}, the white shear bands occur as the result of the further development of the deformed shear bands, as shown in Figure 8(b).[117] This result is confirmed further by the observation in the Al-Li alloys.[77] The results are shown in Figure 9. In other words, a critical strain rate is required, in addition to the critical strain, for the band formation. In fact, the plastic flow is characterized by necking in tension and compression under quasi-static conditions. Under dynamic loading conditions, however, the plastic flow cannot spread uniformly in the whole specimen tested, and is therefore limited in a local region when the strain rate reaches or exceeds a critical value. Table II shows the values of both strain and strain rate needed for the band

Table II. Critical Strain and Strain Rate Required for Shear Formation in Al-Li Alloys

Alloy	Peak-Aged Alloy	Underaged
Strain rate (s^{-1})	1600	2000
Critical strain for the deformed band	0.14	0.17
Critical strain for the white-etching band	0.17	0.21

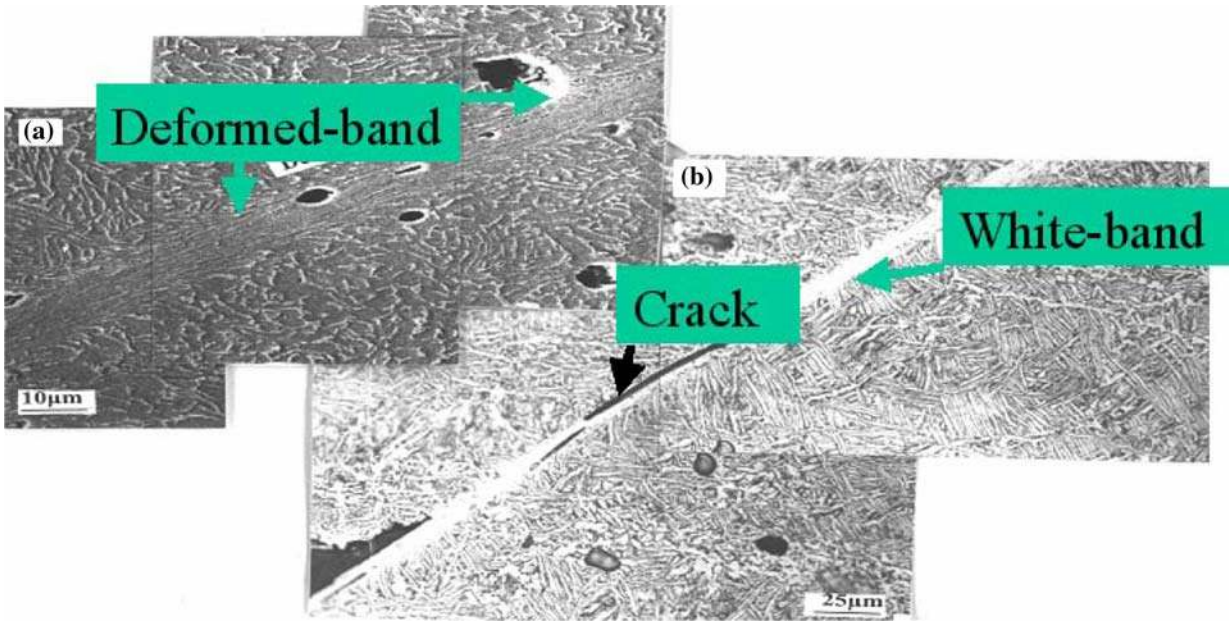

Fig. 8—(*a*) Deformed and (*b*) white-etching bands observed in the titanium alloy subjected to dynamic impact compression loading.

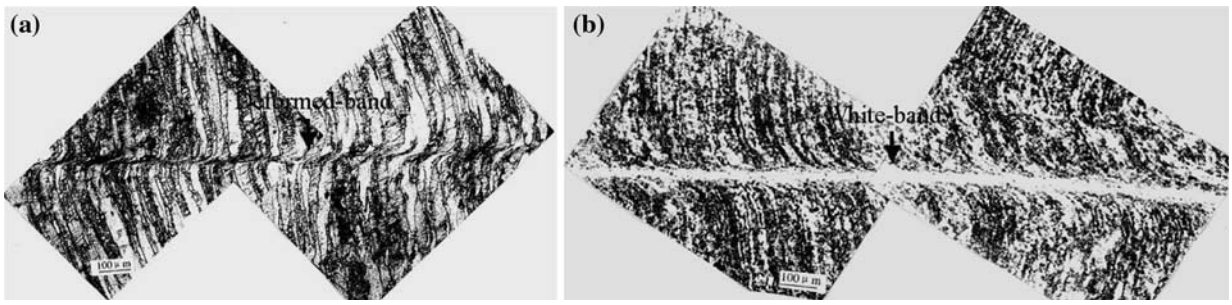

Fig. 9—(*a*) Deformed and (*b*) white-etching bands generated during dynamic impact compression loading in Al-Li alloy.

formation in Al-Li alloys.[77] It is seen that critical strain is 0.14 for deformed shear-band formation, at a given value of the strain rate (1.6×10^3 s^{-1}). After this value, the width of the band decreases with increasing strain. As the strain increases from 0.14 to 0.17, a white-etching band appears (Table II) in the peak-aged alloy. This result is confirmed again by Li *et al.*,[118] who have recently investigated shear-band formation in pure titanium that was subjected to dynamic impact compression. They found that the shear bands began to form when both strain and strain rates reached the critical values of 23 and 2.8×10^3 s^{-1}, respectively.

C. *Deformed and Transformed Bands*

The localized shear bands have been classified as either deformed bands or transformed bands, on the basis of their appearance in metallographic observation.[24,119] The transformed band is often referred to as a white-etching band or a white shear band in steels, and has received much attention, because it is suggested that the phase transformation temperature is reached in the narrow band of material, supporting the thermoplastic instability theory of shear localization. The white-etching bands have been reported mainly in steels (Trent in 1941,[120] Zener and Hollomon,[1] Carrington and Marie in 1948,[121] Andrew *et al.* in 1950,[122] Welsh in 1957,[123] McIntire and Manning in 1958,[124] Rabinowicz in 1965,[125] Scott *et al.* in 1966 and 1967,[126] Nakajima and Mizutani in 1969,[127] Manion and Stock in 1970,[45] Craig and Stock in 1970,[128] Stock *et al.* in 1971,[129] Wingrove in 1971,[130] Glenn and Leslie,[46] Manion and Wingrove in 1972,[49] Thornton and Heiser,[47] Manganello and Abbott in 1972,[131] Eyre and Baxter in 1972,[132] Backman and Finnegan,[110] Wingrove and Wulf in 1973,[133] Woodward and Aghanm,[50] Cho and Duffy,[55] Meyers and Wittman in 1990,[59] and Zurek[115]), and in titanium and titanium alloys (Me-Bar and Shechtman,[33] Timothy and Hutchings in 1985,[34,134] Grebe *et al.*,[29] Timothy,[24] Winter in 1975,[135] Zhou, Rosakis, and Ravichandran in 1996,[136,137] Liao and Duffy,[56] and Xu and Meyers in 2003[138]) and in aluminum lithium alloys (Xu *et al.*[77]).

The evidence for the occurrence of phase transformation in the shear bands in steels seems to rise from the white etch in nital, a well-defined width, distinct boundaries between the band and the matrix, and very high hardness. Trent[120] made the earliest observation of the white-etching bands generated in a plough steel wire that was crushed by a hammer, and found that these bands appeared to be white or slightly yellow on the sheared surface of a wire cut by hand clippers. Using optical metallography, he observed the absence of structure in the white-etching area, attributed any martensitic needles to the deformation-induced transformation, and assumed this must be retained austenite in this high-carbon steel. Some investigators refer to it as a dislocation cell structure, while others refer to it as consisting of extremely fine grains.[46,59] Zener and Hollomon[1] assumed that the white-etching bands were caused by a rapid quenching from the high temperature, and suggested that the strain rates in their punching experiments may have reached 2.0×10^3 s^{-1} and the temperature in the bands may have risen as high as 1000 °C. The hardness of the shear bands led Zener and Hollomon to postulate that they were untempered martensite. Carrington *et al.*[121] have found "white lines" in steel, and they proposed that the heat produced in the white lines probably reach the melting point of material. Andrews *et al.*[122] have studied the white lines in Ni-Cr steel subjected to dynamic impact loading using X-ray diffraction (XRD) techniques, and examined the tempering characteristics of the bands. They suggested that both martensite and austenite may form in the white lines during impact loading, and considered that the austenite may be retained. Their experiments also indicated that the apparent decomposition of the austenite and the accompanying precipitation of carbide usually proceeded from the edge of the white lines. This implied that the center of the white lines could reach a higher temperature than the edges, allowing more complete solution of the carbon and carbide-forming elements. Therefore austenite or martensite at the center of the white lines could be expected to be more stable and, consequently, could be the last temper. However, Scott *et al.*[126] pointed out that the white-etching bands could not show the tempering characteristics of conventional martensite, even when heated to temperatures above normal tempering temperatures; heating to above the austenite temperature, however, could cause a disappearance of the white-etching bands and the formation of a structure indistinguishable from the remainder of the specimen. Based on the selected area electron diffraction (SAED) analysis, they suggested that the white band was supersaturated ferrite, with no resemblance to the normal martensite structure. Further investigations by TEM and X-ray show that the band area is a typical-looking martensite with a high density of dislocation,[59] bct martensite,[47] a fine-grained equiaxed delta ferrite, and a martensite with carbides[139] and untempered martensite.[1] Beatty *et al.*[57] and Meunier *et al.*[58] performed TEM examinations of the white-etching bands and demonstrated that the shear-band region had grains on the order of 20 to 50 nm and was ferritic. However, other structures might form under different conditions.

When we discuss the phase transformation in the bands, the critical role of the temperature rise in phase transformation should mentioned. A number of authors proposed that the maximum temperature rise during localization may reach several hundred degrees above that of the surrounding matrix. This is usually inferred indirectly from metallurgical evidence, and the shear band is then proposed to be rapidly cooled by the surrounding bulk material when plastic deformation ceases, and cooling rates as high as 10^7 K s^{-1} have been calculated.[33] However, some measurements have been made directly by Hartley *et al.*,[40] Marchand and Duffy,[31] Crisman *et al.* in 1989,[140] Duffy and Chi in 1992,[142] Liao and Duffy,[56] and Guduru *et al.*[141] These authors used the IR detection system to determine the temperature distribution of the bands and found that the highest temperature in the band region was in the range of 440 °C to 550 °C for the Ti-6Al-4V

alloys,[56] 450 °C for AISI 1018 cold-rolled steel and AISI 1020 steel,[34] 590 °C for HY-100 steel,[56] and 460 °C for AISI 4340 steel.[143] They concluded, therefore, that there was no clear evidence to suggest that the material within the shear band had undergone a phase transformation. Giovanola pointed out[103] also that there is no conclusive direct evidence for the occurrence of phase transformation in the white-etching bands and that the band structure is not unique; it depends on the deformation history and the original microstructure of the undeformed material. The only important point of common agreement is that the structure in the transformed bands is composed of very fine grains. Rogers mentioned in his review[21] that "whether there is a single crystallographic structure for the transformed adiabatic shear bands in steel or whether there are a variety of structures dependent on the particular material and the deformation condition is still a very open question. There are many indications that the white-etching shear bands may have different structures in different materials and even that the structures may be different in parts of the bands."[22] In addition to etching behavior, there are two almost universally recognized characteristics of the transformed bands in steels: their very high hardness and their extremely fine structure. The investigation made in Al-Li alloys under high-speed impact compression has shown[77] that the deformed bands (Figure 9(a)) form first, corresponding to the critical strain of 0.14, and, as deformation proceeds, localization gradually becomes apparent; finally, the white-etching band occurs on the base of the deformed band, corresponding to a critical strain of 0.17, as shown in Figure 9(b). Timothy pointed out that the formation of a "transformed" shear band appears to correspond to an advanced stage of adiabatic strain localization in a given metal, with a deformed shear band representing an earlier stage in this process.[144] The results mentioned here[55,144] are supported by the recent experimental results in high-speed machining of the high-strength steel.[145]

A number of investigations have demonstrated that whether the bands are deformed or transformed, their presence is generally indicated by the different etching response in a narrow band of material in metallographic cross sections. Figure 10 shows white shear bands observed in 304 stainless steel subjected to explosive collapsed loading. One of the possible reasons for the "white color" of the band is the occurrence of a martensite that is too hard to be etched, causing the white color (the α'-martensite transformation does occur in the band; this will be shown in Section D). In order to verify this, the profile line scanning across the band was

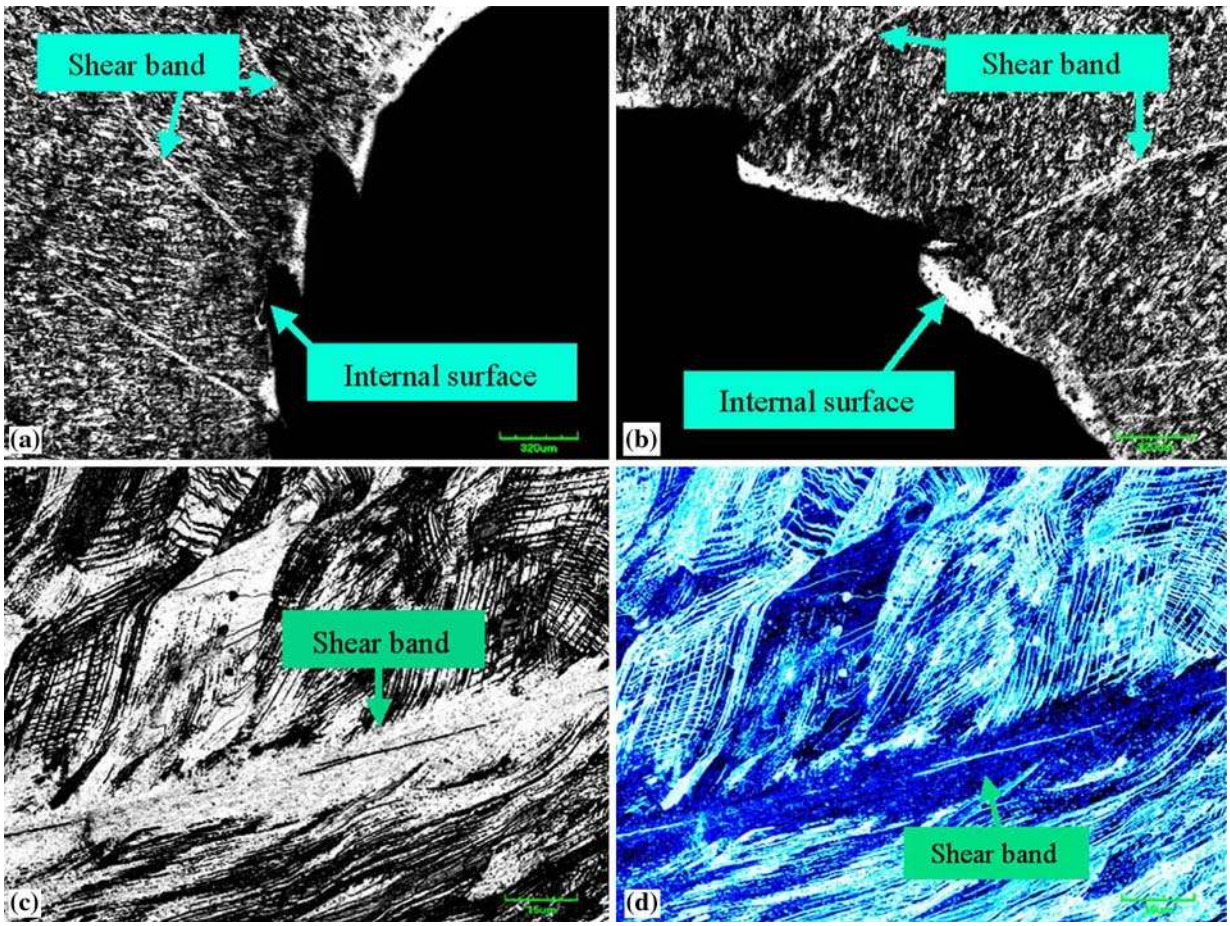

Fig. 10—White-etching shear bands observed in 304 stainless steel subjected to explosive collapsed loading imaged by CFLSM at (*a*) and (*b*) low magnification and (*c*) and (*d*) high magnification.

performed by using CFLSM. If the band is lightly etched, then the profile-scanning line should appear to be protrusion when the scanning is across to the bands (Figure 11). The profile scanning selected is along the horizontal lines (the red lines in Figures 11(c) and (d), respectively). It is seen that the profile-scanning lines do not appear to be protrusion, as shown in Figures 11(c) and (d). This implies that the structure in the band is not difficult to etch. Many investigations show that the structures within the shear bands undergo intensive localized deformation with large strain and super-high strain rate, forming substructures elongated along the shear direction. This is proposed to be the real reason for the white etching color of the band. In other words, the white etching of the bands is an unlikely indication of the phase transformation; in fact, the observed substructures in the white etching differ by a degree not observable by ordinary optical microscopy or by SEM. Both ordinary light waves and secondary electron waves could not "see" the substructure difference in orientation in the bands. Therefore, the band appears to be white when viewed by ordinary light under an optical microscope or secondary electron wave in a scanning electron microscope. So, it is reasonable to propose that the white etching is unlikely to be the occurrence of phase transformation in the bands. This analysis is verified further by recent experimental results in Fe-Cr-Ni monocrystal.[146] Recent investigation has shown however, that phase transformations can occur in both the deformed and transformed bands; these will be described in Section D.

D. *The α′-Martensite Transformation within the Bands*

Recent studies have shown that the phase transformation does occur, certainly in the shear bands in 304 stainless steel[63] and Fe-Cr-Ni monocrystal,[146] and in the Ti-6Al-4V alloys,[84] which were deformed dynamically. Figure 12 shows a shear band and its microstructure observed in 304 stainless steel subjected to the cylindrical collapse (TWC) test with a strain rate of $10^4\ s^{-1}$; Figure 13 is the TEM image taken from a field in the band shown in Figure 12, indicating a α′-martensite phase transformation occurring in the band. This kind of phase transformation particularly generates at the intersection between the shear band and

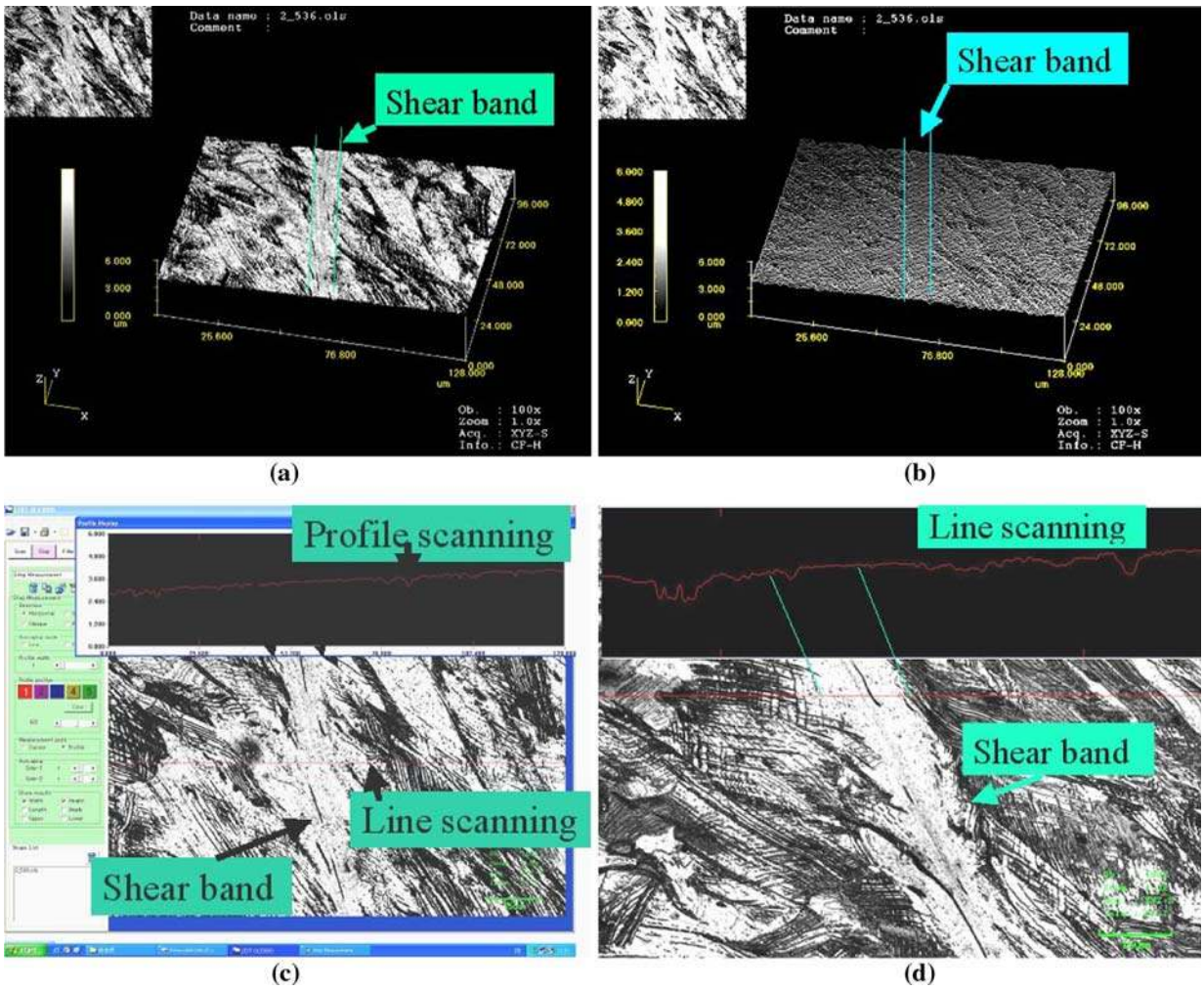

Fig. 11—Profile line scanning across the bands obtained by CFLSM: (*a*) the scanning area, including (*b*) the band, (*c*) area scanning, and (*d*) lines scanning across the band.

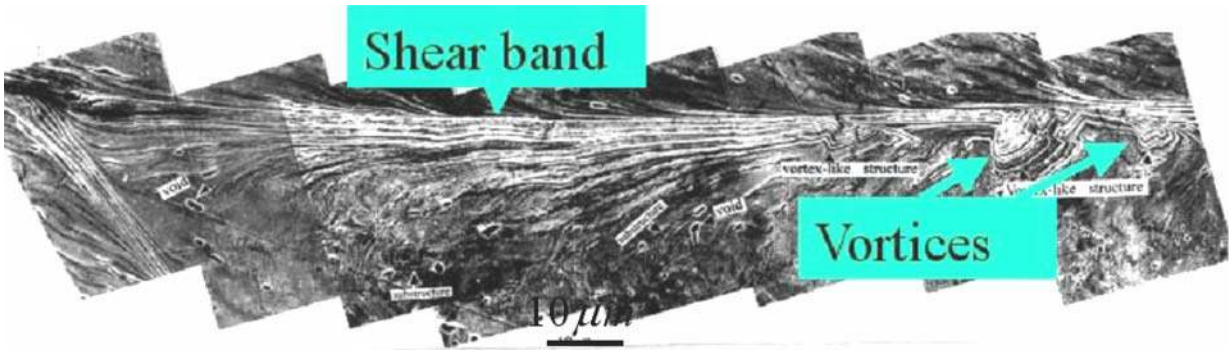

Fig. 12—Shear-band and vortex structure generated in cylindrical collapsed specimen of 304 stainless steel subjected to global $\varepsilon_{ef} = 0.92$.

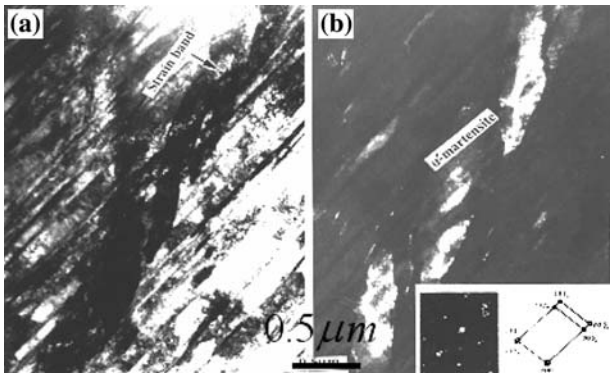

Fig. 13—TEM (*a*) bright- and (*b*) dark-field images, showing α′-martensite phase transformation formed at the intersection between the twins and the shear bands in 304 stainless steel subjected to explosive collapsed testing.

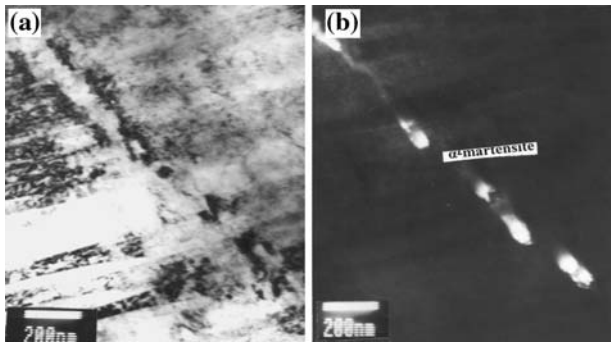

Fig. 14—TEM (*a*) bright- and (*b*) dark-field images, showing that α′-martensite phase transformation appears at the intersection between the twins and the shear bands in Fe-Cr-Ni monocrystal subjected to explosive collapsed testing.

twins, and can be confirmed by dark-field image and electron diffraction analysis. The presence of vortices, also inferred from the IR results by Guduru *et al.*,[141] is also suggested in Figure 12. The dark-field image (Figure 13(b)) is obtained through the appropriate martensite spot, and analysis indicates that the $(\bar{1}10)$ planes of the α′-martensite are coherent with the $(\bar{1}11)$ planes of the parent austenite, and parallel to each other. The direction, [110], of the α′-martensite is parallel to the [211] direction of the austenite, *e.g.*,

$$(\bar{1}\,1\,0)_{\alpha'}//(\bar{1}\,1\,1)_{\gamma}$$

$$[0\,0\,2]_{\alpha'}//[0\,2\,\bar{2}]_{\gamma}$$

$$[\bar{1}\,1\,2]_{\alpha'}//[\bar{1}\,3\,1]_{\gamma}$$

$$[1\,1\,0]_{\alpha'}//[2\,1\,1]_{\gamma}$$

which is the Nishiyama orientation. From this analysis, it is concluded that the (110) of the α′-martensite nucleates along the {111} of the austenite. Essentially, these results confirm an earlier investigation made by Staudhammer *et al.*[147] in dynamic tensile testing of the same materials. These α′-martensite laths nucleate preferentially at twin-band intersections and regions of localized strain. They have been identified by Murr and Ross[148] and Kestenbach and Meyers[149] in connection with shock compression, and by Staudhammer *et al.*[147] in high-strain-rate deformation. These are the twinning and slip planes; thus, their intersections provide the nucleus, as postulated by Olson and Cohen.[150] This kind of phase transformation was also observed within the shear bands in a Fe-15 pct Cr-15 pct Ni monocrystal subjected to the dynamic explosive loading, as shown in Figure 14.[146,151] Figures 14(a) and (b) are bright- and dark-field images of what is presumed to be strain-induced martensite. One more example is shown in Figure 15, indicating that the phase transformation also occurs in the deformed-type bands in the Ti-6Al-4V alloy. Figure 15(a) is a bright-field image taken from a primary-α grain of the alloy, and Figure 15(b) is its combined electron diffraction pattern. Figures 15(c) and (d) are the bright- and dark-field images that were obtained by the strong diffraction (α) and the weak superlattice reflection $\{1\bar{1}00\}_{\alpha 2}$, respectively. According to the analyses of the electron diffraction and dark-field image, the α_2 phases (Ti_3Al) are proposed to be transformed from the α matrix, and both the α_2 phases and α matrix are completely coherent. This kind of transformation is proposed to be, to the authors'

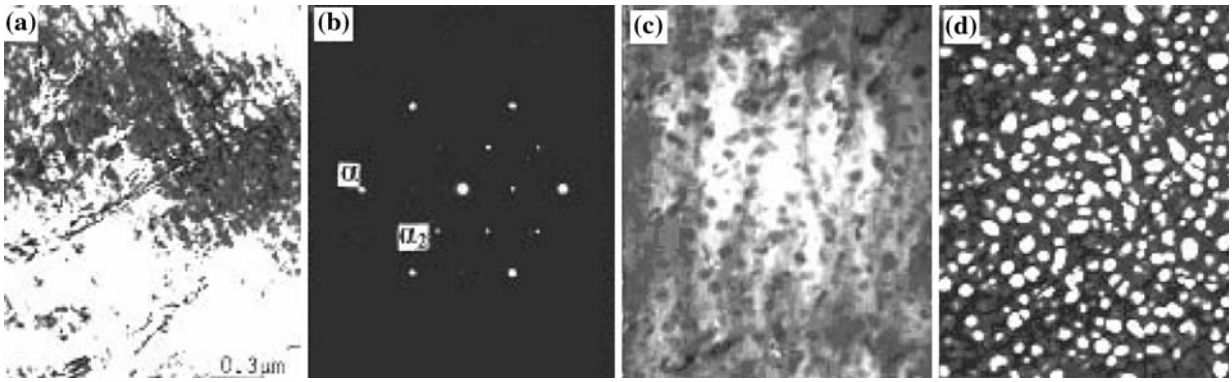

Fig. 15—TEM montage, showing (*a*) bright-field of the high-strain-rate deformation structure in Ti-6Al-4V alloy, and its (*b*) [0001] zone axis diffraction pattern and dark-field images obtained by using strong diffraction spots $\{2\bar{2}00\}_{\alpha}$ marked by α and weak superlattice reflection $\{1\bar{1}00\}_{\alpha 2}$ marked by α.

knowledge, the first finding in this alloy subjected to explosive collapsed loading.

The $\alpha \rightarrow \alpha_2$ (Ti_3Al) transformation has been reported in the titanium-alloys.[152–155] Mendiratta *et al.*[152] have reported the α_2 (Ti_3Al) precipitation in Ti-6Al-2Sn-4Zr-2Mo during creep, and found that the α_2 (Ti_3Al) particles are extremely small and, therefore, are likely to be sheared by the dislocations in the α matrix.[153] Li *et al.*[154] investigated formation of the Ti_3X (where X = Al, V, and Zr) phases in titanium alloy, and found that when the content of X in the alloy reaches a critical solution degree, the long-region ordered phase (Ti_3X) with superlattice structure starts to occur in α-Ti.[123] The shape and distribution of the α_2 phases they obtained are similar to the observations in the present investigation. However, the transformation from α to α_2 in the Ti-6Al-4V alloy induced by dynamical deformation under a high strain rate has not been published, and further studies for mechanism of the phenomenon are still needed.

The occurrence of martensitic transformation in concurrence with shear-band formation has been demonstrated[151] in a Fe-Ni-C monocrystal. The spacing of shear bands was affected by the presence or absence of martensite. Meyers *et al.*[151] demonstrated that there are interaction effects between martensite transformation and shear-band propagation.

E. *Effect of the Microstructures on Shear-Band Formation*

It is generally accepted that a material will be sensitive to localized shearing if it is characterized by a low strain hardening, a low specific heat, and a high thermal softening. Rogers pointed out[21,22] that the deformed bands are likely to form in iron, in low-carbon steels, and in higher-carbon steels, when the structure is coarse. Also, as the rate of deformation decreases, there is a greater tendency for the shear bands to be of the deformed type, and a transformed portion to extend from the region of most intense shear to a point at which the local temperature has not exceeded the transformation temperature. Rogers and Shastry proposed[119] that the transformed band may be partly along the adiabatic band and partly along the deformed band for the remainder, and that the type of band forming is highly dependent on the specific deformation conditions. Backman and Finnegan[110] studied the tendency of several different metallurgical structures in AISI 4130 steel to the formation of the different types of the bands during ballistic impact and found that, when the steel was heat treated to produce either pearlite or Widmanstätten ferrite, only deformed bands were observed; when the steel was heat treated to produce a tempered martensitic or lower bainitic structure, the white-etching transformed bands were formed. It can be seen that the effects of the material structures on localized shearing have not been well understood. Costin *et al.*[156] have found that the localized shear band developed in all high-strain-rate tests with cold-rolled steel, and that none forms in hot-rolled steel when deformation is limited to about 30 pct strain; these two steels have similar chemistries and showed very similar strain-rate sensitivities and thermal softening rates. However, Shawki and Clifton[157] predicted that the shear bands would form in hot-rolled steel, deforming dynamically if a nominal strain of 80 to 100 pct were imposed; they have considered that the reason no localized shear formed in the hot-rolled steel may be attributed to the low strain used. This proposal was justified by the results of Hartley *et al.*[158] However, they found that the shear bands in hot-rolled steel (about 150 μm wide) are narrower than that in cold-rolled steel (about 250 μm wide). Xu *et al.*[44,159–161] studied the tendency of the low-carbon steels with different structures to shear localization and found that the critical strain required for the occurrence of shear localization is strongly dependent on the strength at a given strain rate. This can be seen clearly from Figure 16, which shows that the critical strain values for the quenched, quenched and tempered, and normalized steels are 0.30, 0.36, and 0.83, respectively, implying that the steel with quenched martensite is most susceptible to shear localization. The higher the strength of the steels, the easier it is for the shear band to occur. The quenched steel with high strength and low work-hardening capability does

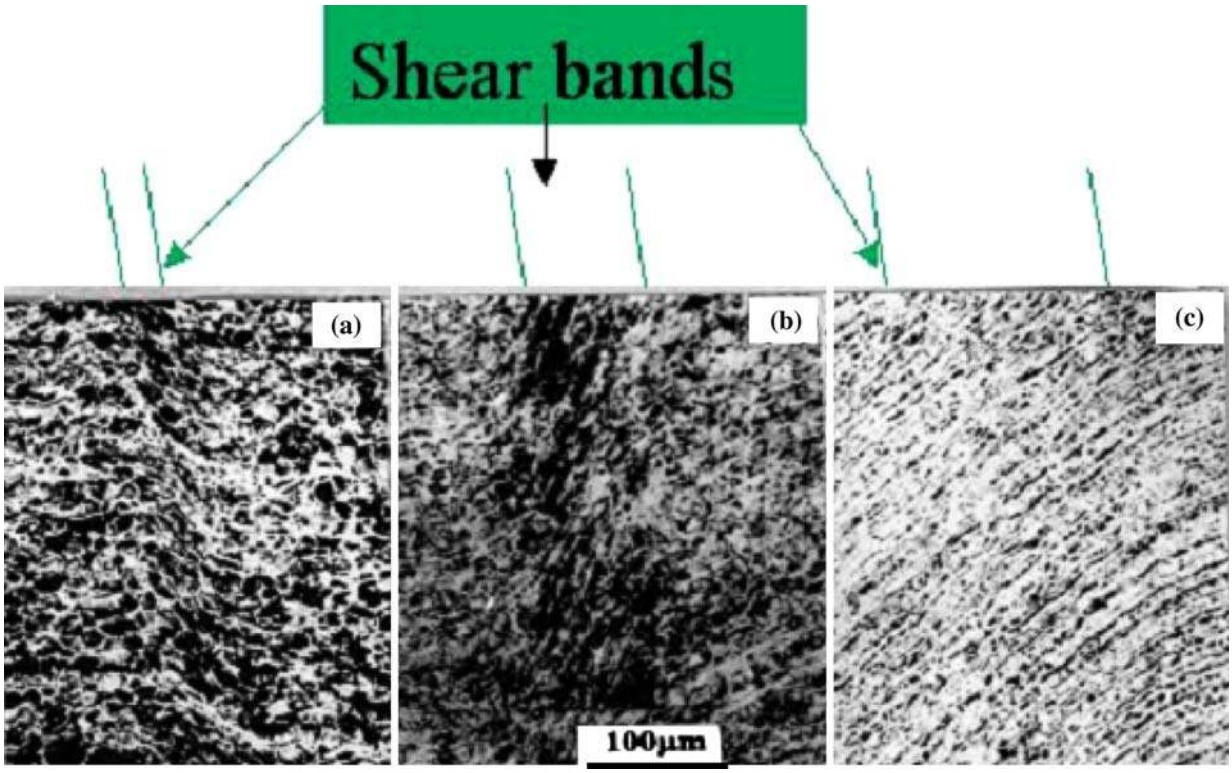

Fig. 16—Localized shear bands in the low-carbon steels: (*a*) quenched condition, (*b*) quenched and tempered, and (*c*) normalized.

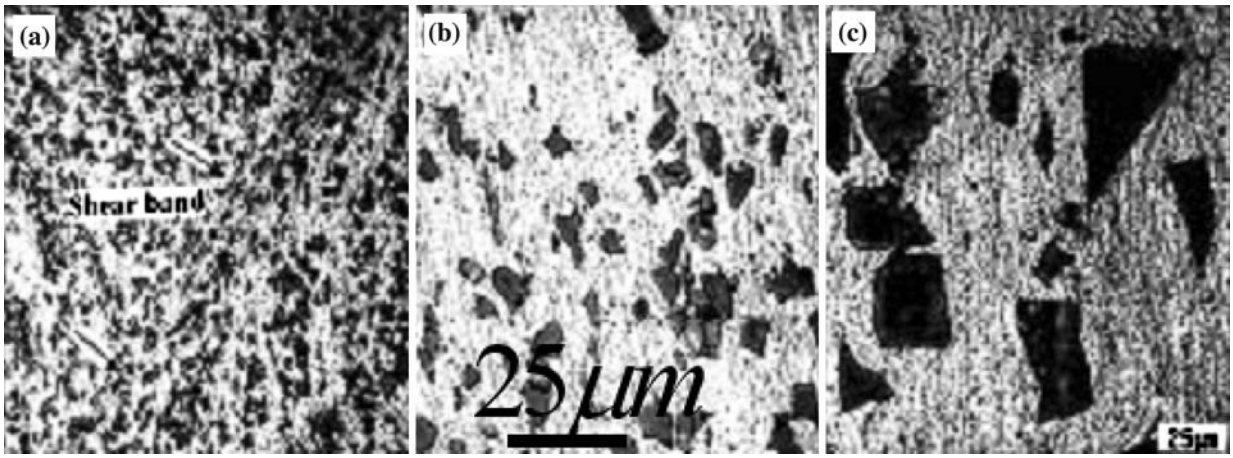

Fig. 17—SEM montage, showing deformation pattern in Al-17 pct SiC_p composite with an average particle size of (*a*) 3, (*b*) 13, and (*c*) 17 μm, produced during high-strain-rate loading. Note that material with smaller particles (3 μm) develops a well-defined localized shear band (a), and shear localization in the materials with larger particles (13 and 17 μm) does not develop well.

develop pronounced shear bands with a width of 70 to 100 μm (Figure 16(a)). However, the width of the bands in normalized steel with a higher capability of work hardening is much larger than those of the other two steels, approximately 350 to 400 μm (Figure 16(c)). The width in the quenched and tempered steel is in between them (Figure 16(b)). It should be pointed that the boundary between the bands and the steel matrix for these steels is not well defined.

One more example is shown in Figure 17, displaying the effect of the microstructure on the tendency for localized shear deformation in the aluminum matrix composites reinforced with different size SiC particles.[162] It is found that the composite reinforced with smaller particles (3 μm) develops well-defined shear bands, as shown in Figure 17(a), and those with larger SiC_p, 13 and 17 μm in size, tend to deform inhomogeneously, so localized shear was not well developed, as shown in Figures 17(b) and (c). This implies that the particles may play a significant role in the formation and development of shear localization, and the smaller the size of the particles in the composites, the easier the

shear-band formation; this coincides with the results obtained by Lee *et al.*[163,164] and Ling and Luo *et al.*[165,166] The tendency of the composite reinforced with small particles to form shear localization is greater than that of other two materials with large particles, when the volume fraction of the particles in the composite remains the same. This size-dependent deformation localization behavior of particle-reinforced metal matrix composites is confirmed by recent research results.[167,168]

F. *Amorphous Phase within the Bands*

It is remarkable that an amorphous region in the shear bands was recognized in the TWC specimens of both 304 stainless steel and Fe-Ni-Cr monocrystal that were subjected to explosive collapse loading.[63,146] The observation in monocrystalline Fe-Cr pct Ni under the same experimental conditions as the observation in AISI 304 stainless steel described by Meyers *et al.*[151] is shown in Figure 18. It can be seen that the interface between the amorphous and the crystalline regions is clear, that the amorphous region is absent from the crystalline lattice, and that the crystalline region is composed of the nanograins. Figure 19 shows HREM images taken from these two different regions in Figure 18. It is clear that some small, nanometer-sized zones retained lattice fringes (Figure 19(a)), which were distributed over the whole amorphous area (Figure 19(b)). These observations were further confirmed by HREM conducted on 304 stainless steel and shown in Figure 20, where one can note that some areas are not transformed into the amorphous phase and retain the lattice fringe feature (Figure 18). The absence of imaging from the crystalline lattice, in contrast with the crystalline region, is strong evidence for the lack of crystalline symmetry. This is a surprising finding and is,

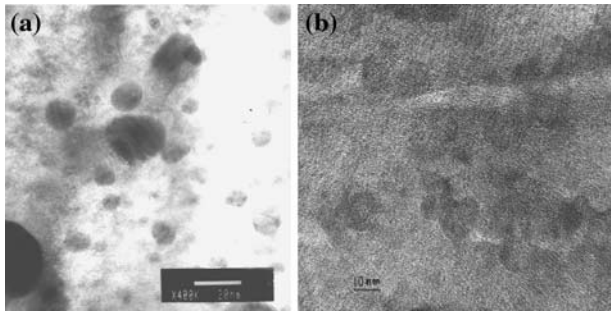

Fig. 19—HREM images, showing (*a*) nanosized grains and (*b*) amorphous phase in the shear band produced during explosive collapsed loading.

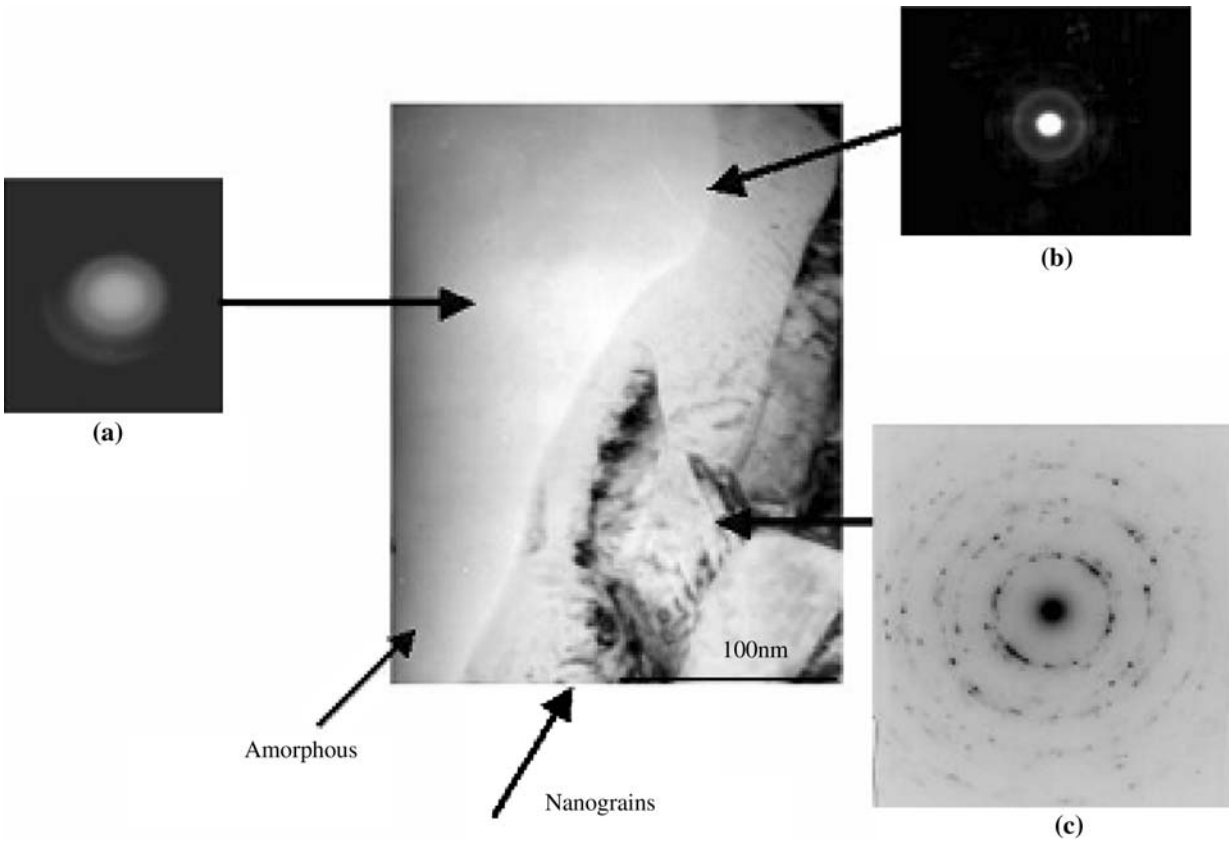

Fig. 18—TEM (bright-field) image taken from a region in shear band showing the amorphous phase and nanocrystalline regions, and corresponding diffraction patterns from the (*a*) amorphous phase, (*b*) nanocrystalline region, and (*c*) interface of nanocrystalline and amorphous phase in Fe-Cr-Ni crystal subjected to TWC collapse.

to the authors' knowledge, the first observation of a crystalline-to-amorphous transition in a localized shear band. This kind of transformation of a crystalline-to-amorphous state has been observed in many binary alloy systems by mechanical alloying[169–171] and by ball milling.[172–175] In the former case, the results show that a negative heat of mixing and last diffusion of one of the elements favor the formation of an amorphous alloy phase[176] and, in the latter case, ball milling may induce not only the accumulation of lattice and point defects but also chemical disordering in the lattice. If the rate of dynamic recovery is lower than the rate of defect production, the accumulation of these topological and chemical disorders may lead to a collapse of the crystalline structure.[169] Meyers *et al.*[63] have proposed a reasonable explanation for this solid-state amorphization and considered that the transition of crystalline-to-amorphous phase in the case of the shear localization is completely possible.[63]

It should be pointed out that there is a possibility that the amorphous phase could be induced by ion milling during thin-foil preparation for TEM examination. Several points should be noted. First, as shown in Figure 19, only an isolated amorphous region is observed around the hole; if it is induced by ion milling, then the amorphous regions should be distributed along the edge of the hole. Second, there is clear interface between the amorphous and nanograin regions, and their arrangement alternates from one to another, as shown in Figure 18. If it is caused by ion milling, there is no possibility for the amorphous regions to show this type of alternative arrangement. Third, some nanograins, 10 nm in diameter, are distributed over the amorphous region (Figure 20), and some zones still retain low-dimensional lattice fringes (Figures 20(a) and (b)), implying that the transition of the crystal lattice to amorphous matter is not complete. The distribution of amorphous regions should be homogeneous, if it is introduced by ion milling. Therefore, it is reasonable to consider that the amorphous matter observed within the shear bands in the present study should be the product of transformation from crystalline-to-amorphous domains during localization.

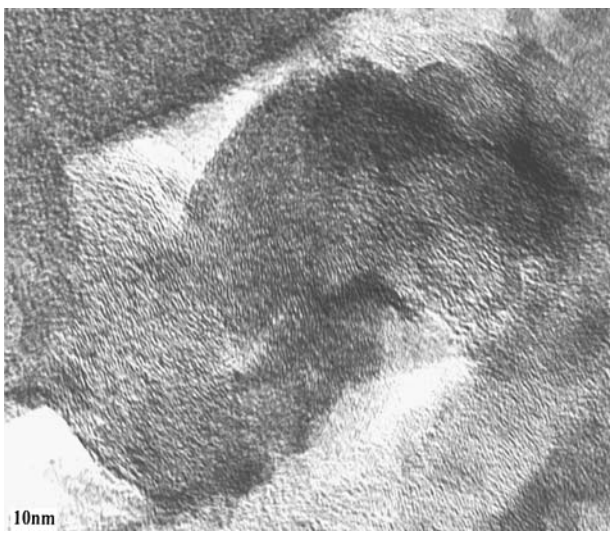

Fig. 20—HREM image taken from the amorphous region in the shear bands in 304 stainless steel produced during explosive collapsed testing. Note that some zones still keep two-dimensional lattice fringes.

G. *Recrystallization*

Recrystallization arising from high-strain-rate loading has been well documented by some investigators in steels (Glass and Moss in 1961,[177] Mataya and Carr in 1982,[178] Meyers and Xu,[63] Li *et al.*,[179] Lins *et al.*[180]), in titanium (Meyers and Pak in 1986,[35] Xu and Meyers in 2003,[138] Chichili *et al.*[38]), in copper (Andrade *et al.* in 1994,[181] Hines and Vecchio in 1995,[182] Murr *et al.* in 1995,[183] and Hines *et al.* in 1998,[184]), in tantalum (Pappu *et al.* in 1995,[185] Murr *et al.* in 1994,[186] Nesterenko *et al.* in 1997,[187] Meyers and Chen in 1995,[43,73] and Nemat Nasser *et al.*[75]), in aluminum-lithium alloys (Xu *et al.*[77] and Meyers *et al.* in 2000[187,188]), in Al/SiC_p composites (Xu *et al.*[162]), and in Ni-Cu alloys (Li *et al.* in 2000[189]). It is generally accepted that the deformation and associated temperature rise during high-strain-rate loading are, therefore, sufficient to produce new recrystallized grains in the shear bands, although it is not clear at present that this recrystallized microstructure develops simultaneously with deformation (dynamic recrystallization (DRX)) or subsequent to deformation (static recrystallization). The microstructural characteristics of DRX are the fine equiaxed grains with low dislocation density and well-defined grain boundaries. Glass *et al.*[177] made the earliest observation of recrystallization in shear bands in an explosively loaded steel cylinder; they surmised that the fine undeformed grains were the result of recrystallization. Based on dislocation dynamics and subgrain-boundary change in orientation enhanced by plastic deformation, Li *et al.*[179,189] and Meyers *et al.*[190] independently proposed models for describing this DRX, which occurs during high-strain-rate deformation.

Cho *et al.*[191] considered that the fine equiaxed grains observed in the center region of a shear band in HY-100 steel was caused by dynamic recovery rather than by DRX. It is possible that, in their case, the strain inside the shear band was not sufficient to complete the recrystallization process.

Recent investigations show that this recrystallization also occurred in 304 stainless steel[63] and Ti-6Al-4V alloy[138] subjected to explosive collapse loading. Figure 21(a) shows a bright-field image consisting of nanograins with an average size of 100 nm in diameter, within a band of 304 stainless steel. For comparison, both large grains approximately 50 to 100 μm in diameter located external to the band region and the high density of dislocations are illustrated in Figure 21(b). There are several prominent features of microstructural change between intraband regions and extraband regions (Figures 21(a) and (b)). The size of the refined grains within the band (Figure 21(a)) is much smaller, by 10 orders of magnitude, than the grains with profuse dislocations outside the band (Figure 21(b)). The second feature is the absence of deformation twins

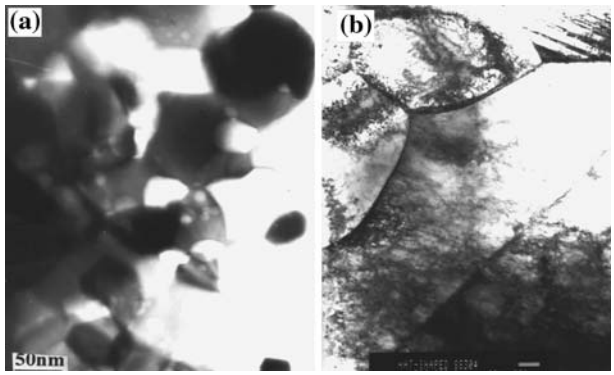

Fig. 21—Nanograins (50 to 100 nm in diameter) (a) inside deformed bands and large grains (50 to 100 μm) with high density of dislocations outside bands.

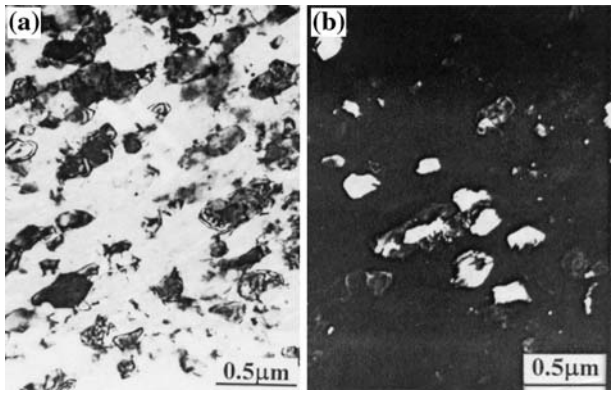

Fig. 22—(*a*) Bright- and (*b*) dark-field TEM showing ultrafine-grain-sized structure within shear band in Al-Li alloy.

within the bands while the density of dislocation is high outside the band. A similar phenomenon was also observed in the Al-Li alloy subjected to shear localization. Figure 22(a) shows a bright-field TEM of distortion-free and equiaxed grains taken from a shear band in this alloy, whereas Figure 22(b) shows the dark-field image. These new grains (~200 nm) in the bands are much smaller in size, by factors of 10 to 100, than the grains outside the bands. All these features observed within the shear bands in 304 stainless steel and Al-Li alloy are indicative of recrystallization that occurs in the shear bands during localized shear deformation.

Figure 23 shows four different metals in which the shear localization region exhibits the same features: equiaxed grains with diameters on the order of 100 to 4000 nm. They represent the fcc (copper and 304 stainless steel), bcc (interstitial-free (IF) steel), and hcp (titanium) structures. The microstructures for these different crystal structures (hcp, fcc, and bcc) are remarkably similar: approximately equiaxed micrograins with diameters between 0.1 and 0.3 μm.

The structure shown in Figure 23(d) represents an electron backscattered diffraction (EBSD) of a forced shear band in IF steel. Lins *et al.*[180] propose a subgrain-progressive, subgrain-misorientation recrystallization similar to the rotational recrystallization proposed earlier by Meyers *et al.*[190] The results presented herein are in full agreement with the early observations through TEM by Grebe *et al.*[29] in Ti-6Al-4V and by Meyers and Pak[35] and Meyers *et al.*[36] on commercial-purity titanium. Results by Chichili *et al.*[38] also show the formation of an equiaxed ultrafine-grained structure inside the shear band in Ti. Indeed, the response of Zr is very similar to Ti, including the shear-band width.

Figure 24 depicts a well-defined shear band in Zircaloy.[68] The shear-band interface cuts the picture diagonally (Figure 24(a)). A very refined microstructure is apparent. This microstructure is seen in greater detail in Figures 24(b) and (c). In spite of the large deformation applied, the final grain size within the band is approximately 200 nm. The selected area diffraction pattern (SADP) corresponding to the ultrafine-grained structure developed within the band, illustrated in Figure 24(d), consists of well-defined rings, indicating the presence of highly misoriented grains. It should be noted that the diffraction pattern was taken using an aperture size large enough to encompass the entire band width.

Derby[192] proposed two kinds of mechanisms (rotational and migrational types) for the DRX produced under a high strain rate. Because the time required for formation of the shear band is lower by several orders of magnitude than the time required to create grains of the 0.1-μm size by the migration of the boundaries,[189,193] conventional migrational recrystallization could not be considered to be the mechanism of DRX. However, a number of investigations show that a variety of dislocation sources, including the Frank–Read source, will be activated and, therefore, dislocations are multiplied significantly under dynamic loading. Campbell *et al.*[194] have pointed out that a typical Frank–Read source will begin to be multiplied in 5×10^{-9} μs and, at that time, the estimated plastic strain in a typical metal will be only 0.003. These dislocations will form substructures such as cells and tangles, leading to heterogeneous distribution in microstrain in the shear bands, while the temperature increases simultaneously. These could provide favored conditions for the nucleation of new grains. Because deformation and recrystallization in the bands proceed simultaneously during localization, the new grains and deformation features within the recrystallized grains could sometimes be observed. However, if the temperature in the bands decreases very quickly due to thermal diffusion, the residual deformation structures can be kept and, therefore, the new recrystallized grains could hardly be observed in this case, depending on the materials tested. The dislocation multiplication and formation of the cells in the bands are like a first step in DRX, and then the difference in orientation of the sub-boundaries increases, because a great deal of dislocation is absorbed into the subgrain boundaries under high-rate deformation and, finally, sub-boundary rotation may take place during localization, leading to nucleation of the new grains in the shear bands. The calculation demonstrates that DRX will be a spontaneous production process from the point of transition from high to low energy.[187,195]

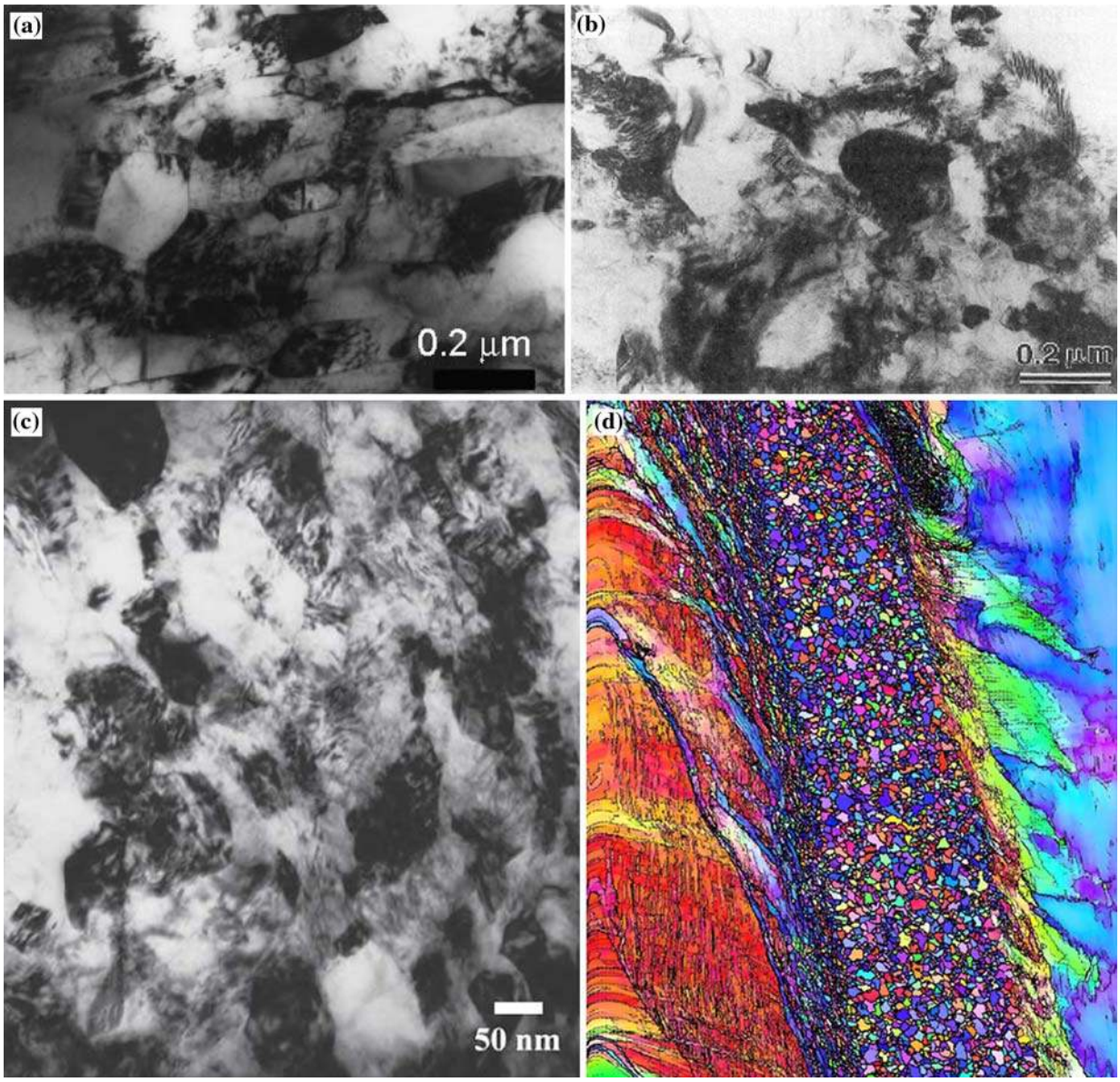

Fig. 23—Ultrafine-grained structure in bands in (*a*) copper, (*b*) titanium, (*c*) stainless steel (courtesy of E. Cerreta), and (*d*) interstitial-free steel (courtesy of K.S. Vecchio).

The sequence of events depicted in Figure 25 is expected to occur. It was first postulated by Andrade *et al.*[181] and Meyers *et al.*,[190] and has since then been described in increasing detail. In essence, one starts with a random dislocation distribution (Figure 25(a)), which is not a low-energy configuration. This random distribution gives way to elongated cells. This stage is shown in Figure 25(b). As the deformation continues and the misorientation increases, these cells become elongated subgrains (Figure 25(c)). These elongated structures are seen in many metals subjected to high strains, as reported by Gil Sevillano *et al.*,[197] among others. Hughes and Hansen[198] reported rotations of 30 to 45 deg at medium and large strains (cold-rolling reductions from 70 to 90 pct). Hughes *et al.*[199] made detailed TEM observations on heavily deformed metals Ta and found evolution from configuration (b) to (c) in Figure 25. These elongated subgrains are, in their turn, plastically deformed, leading to further breakup (Figure 25(d)). Eventually, the elongated subgrains break up into approximately equiaxed micrograins (Figure 25(e)).This sequence of events, which is well known for severe plastic deformation (SPD), has received different names:

(a) rotational DRX (*e.g.*, Derby[192]), which needs concurrent plastic deformation; it is well documented for geological materials (this was the interpretation given by Meyers *et al.*[36] for titanium, Andrade *et al.*[181] for copper, and Nesterenko *et al.*[187] for tantalum);
(b) formation of geometrically necessary boundaries;[200]

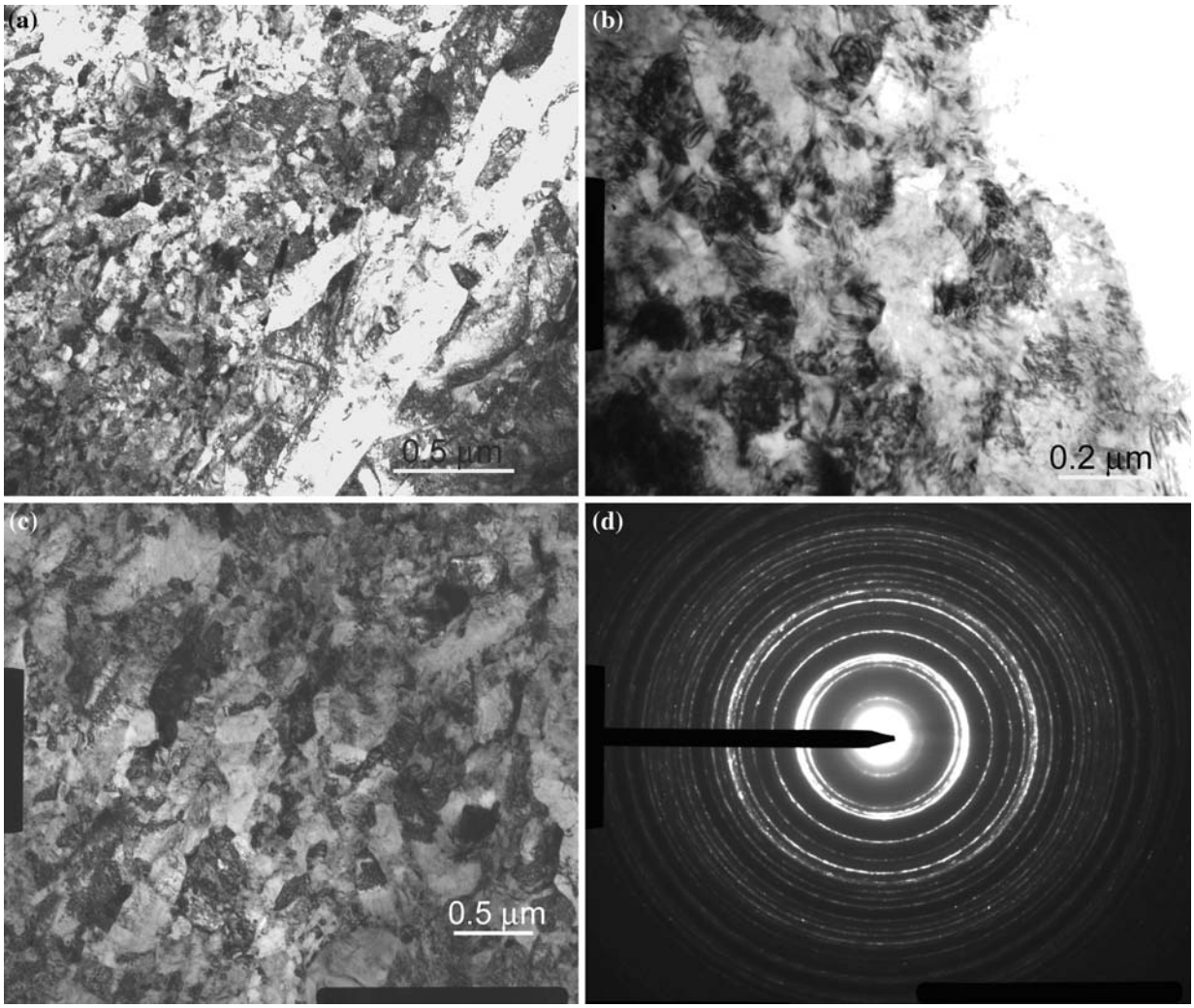

Fig. 24—Zircaloy hat-shaped specimen: (*a*) interface between shear band and adjacent regions, (*b*) and (*c*) interior of the shear band, (*d*) SADP corresponding to the ultrafine-grained microstructure (courtesy of B. Kad and A. Mishra, University of California at San Diego).

(c) continuous recrystallization;[201] and
(d) progressive subgrain misorientation recrystallization.[180]

Once this equiaxed ultrafine-grained structure is achieved, it has to undergo additional plastic deformation under the imposed conditions. Due to the difficulties encountered in measuring the temperature rise inside the band during dynamic loading, the temperature within the band has to be estimated; here, we will give a simple method for the calculation of the temperature rise in the band that was performed on a 2024Al/SiC_p composite.[162] The temperature that makes the onset of thermal recovery or recrystallization in metals is generally expressed by

$$T = (0.4 - 0.5\ T_m) \qquad [1]$$

where T_m, the melting point of metals, is 933 K for the Al alloy. Therefore, if recystallization occurs in the Al alloy, the temperature in the band should be in the range of 373 to 466 K. We assumed that most of the plastic deformation work is converted into heat (90 pct). Thus, the temperature rise in the band can be estimated using the stress-strain response from the same material in the cylindrical compression test (Ling and Luo[166]), and expressed by

$$T = T_o + 0.9 W_p/\rho \cdot C_v \qquad [2]$$

where T_o is the room temperature; C_v, the heat capacity, is 903 J/Kg k for Al; the density of the material is 2.7×10^3 kg/m^3; and W_p, the specific work of deformation, can be expressed by the following equation:

$$W_p = \int \sigma \cdot d\varepsilon \qquad [3]$$

Assuming linear hardening up to a strain of 0.56 for the 2124Al/SiC_p composite, we obtained $W_p = 560 \times 106$ J/m^3, according to the data in the literature (Ling and Luo[166]). Thus, the temperature rise in the band is

$$T = T_o + 0.9\ W_p/C_v = 293\ \text{K} + 206\ \text{K} = 499\ \text{K} \qquad [4]$$

which is higher than the recrystallization temperature in Al (373 to 466 K). This calculation for the temperature

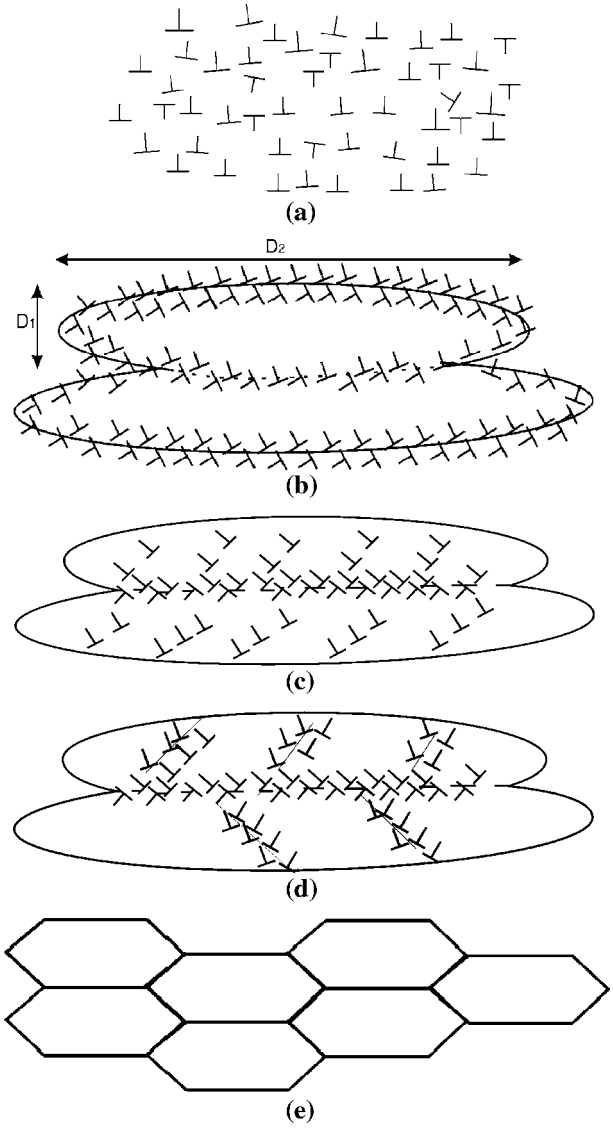

Fig. 25—Schematic illustration of microstructural evolution during severe dynamic plastic deformation: (*a*) homogeneous distribution of dislocations, (*b*) elongated cell formation, (*c*) dislocation accumulation in subgrain boundaries, (*d*) breakup of elongated subgrains, and (*e*) reorientation of subgrain boundaries and formation.

rise in the band is coincident with that of the Al-Li alloy (Xu *et al.*[77]). Similarly, the temperature outside the band is estimated to be 402 K, which is lower than that of recrystallization. This simple calculation is in good agreement with the experimental observation of the present study, and it is reasonable to propose that the observed equiaxed grains result from the occurrence of recrystallization in this material.

H. *Grain Rotation Mechanisms and Similarities with Equichannel Angular Processing*

A possible mechanism is presented in this section. It was proposed for SPD, an emerging area of research for the production of ultrafine-grained metals. It is described in detail by Mishra *et al.*[222] and Kad *et al.*[68] As the grain size is reduced to the range of 50 to 200 nm by the localized deformation in the shear band, the deformation mechanisms operating at conventional grain sizes have to be re-examined. This is an area of intense current research, and the concept of grain-boundary sources and sinks is gaining importance.[93,113] We assume that grain boundaries act as primary sources of dislocations. There is an associated shear of the idealized cubic ultrafine grain. When the dislocations are annihilated in the opposite boundary, the cube is transformed into a parallelepiped.

The deformation temperature is such that grain-boundary rotation is possible within the deformation process. This rotation of the grain boundaries, coupled with shear on a new slip plane, ensures the retention of a steady-state equiaxed structure. The process of grain-boundary rotation during deformation was first analyzed by Meyers *et al.*[42] and extended to severe plastic deformation (SPD) by Mishra *et al.*[222] It is reproduced here in a succinct fashion. In order for this mechanism to be viable, it has to be shown that grain-boundary rotation can be accomplished in this short deformation time. The relaxation of the rotated grains into a more equiaxed microcrystalline structure can occur by minor rotations of the grain boundaries. This is shown in Figures 26(a) and (b), where it is shown that a rotation of 30 deg of the boundaries transforms elongated, segmented subgrains into an equiaxed structure. If each longitudinal grain-boundary segment AB rotates to A′B′ by an angle θ, the original equiaxed structure will be created. This is illustrated in Figures 26(a) and (b). This can be accomplished by the flux of atoms along the grain boundary, which can occur at rates that are orders of magnitude higher than in the bulk. The activation energy for grain-boundary diffusion is approximately one half of that for the lattice diffusion and, at $T/T_m = 0.5$, the ratio between grain-boundary diffusion, D_{GB}, and lattice diffusion, D_L, is between 10^7 and 10^8.[203]

The rotation of the boundaries is driven by the minimization of the interfacial energy (*e.g.*, Murr[96]).The force exerted by the grain boundaries is equal to (= 180 deg)

$$F = \gamma\left(1 - 2\cos\frac{\theta_0}{2}\right)L \qquad [5]$$

where γ is the grain-boundary energy, L is the length of the grain-boundary segments shown in Figure 26, and θ_0 is the initial value of the angle between the boundaries.

The final expression for the angle of rotation θ as a function of time, t, is

$$\frac{\tan\theta - 23\cos\theta}{(1 - 2\sin\theta)} + \frac{4}{3\sqrt{3}}\ln\frac{\tan\theta 2 - 2 - \sqrt{3}}{\tan\theta 2 - 2 + \sqrt{3}} + \frac{2}{3} - \frac{4}{3\sqrt{3}}\ln\frac{2+\sqrt{3}}{2-\sqrt{3}} = \frac{4\delta D\gamma}{L_1 kT}t \qquad [6]$$

A detailed derivation is provided by Meyers *et al.*[208] The term D is the grain-boundary diffusion coefficient and δ is the thickness of the grain boundary. In Figure 27, the grain side $L_1 = 0.2$ μm. This is a conservative value, since a hexagonal grain with diameter of

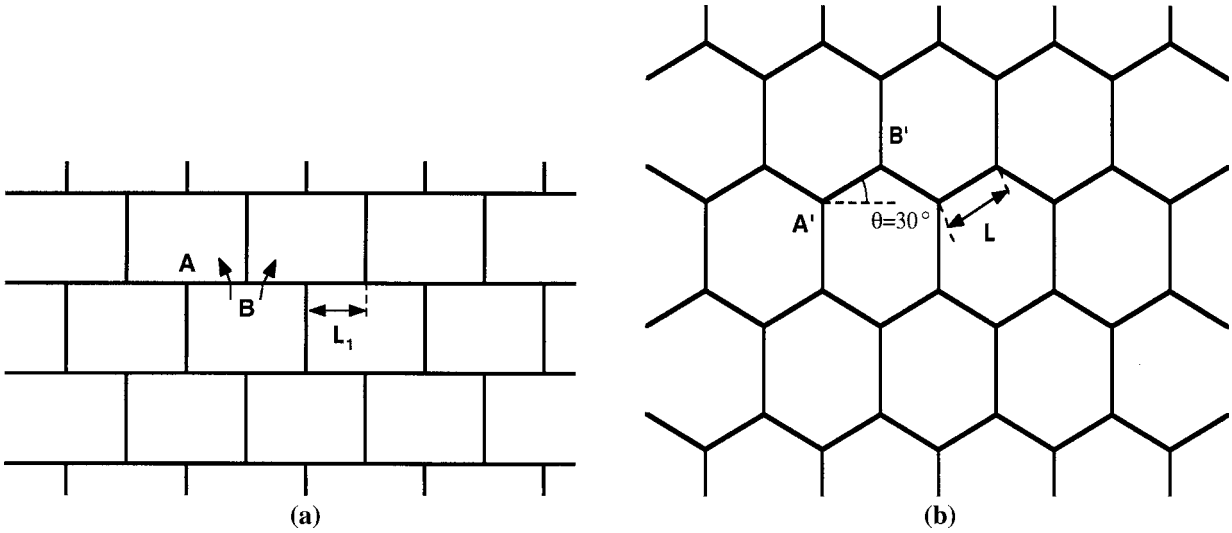

Fig. 26—(*a*) Original configuration of subgrains after breakup and (*b*) rotation of boundaries leading to equiaxed structure.

0.2 μm would have a side of 0.1 μm. The most important parameter in Eq. [6] is the grain-boundary diffusion coefficient. The grain-boundary width is variously taken as 0.5 to 1 nm. The interfacial energy was obtained from Murr.[209] It is taken as 0.725 mJ/m^2. The rate of rotation decreases with increasing θ and asymptotically approaches 30 deg as $t \rightarrow \infty$. The calculations predict significant rotations of the boundary within the deformation time (~50 to 100 μs) at temperatures between 0.45 and 0.5 T_m, for micrograin sizes of 0.1 to 0.3 μm. Thus, the reorientation of grain boundaries can take place during plastic deformation. This does not exclude the possibility of the reorientation or accommodation of the grain boundaries during cooling.

The rotation as a function of time is shown for T = 0.4, 0.45, and 0.5 T_m in Figure 27(a), which is directed at the shear band. It can be seen that the grain boundaries can rotate at times on the order of 20 ms. This is on the order of the deformation time. Thus, an equiaxed structure can be achieved in copper. For equichannel angular processing (ECAP), the situation is quite different: the temperature rises per pass are much more modest (~50 to 70 K) (Figure 27(b)). Thus, the times are much longer, but still in the realm of the extrusion process: ~0.1 second. It is interesting to note that both processes have, in spite of dramatic differences in strain rate and temperature, fairly similar Zener parameters ($\ln Z = \ln \dot{\varepsilon} + Q/\mathrm{R}T = 35$)

I. *Super-High-Strain-Rate Deformation within the Bands*

It is well known that, once localized shear deformation has commenced, a steep strain and strain rate as well as temperature rise will appear in the shear bands. Li[196] made an interesting observation and has calculated the deformation behavior of the white band in

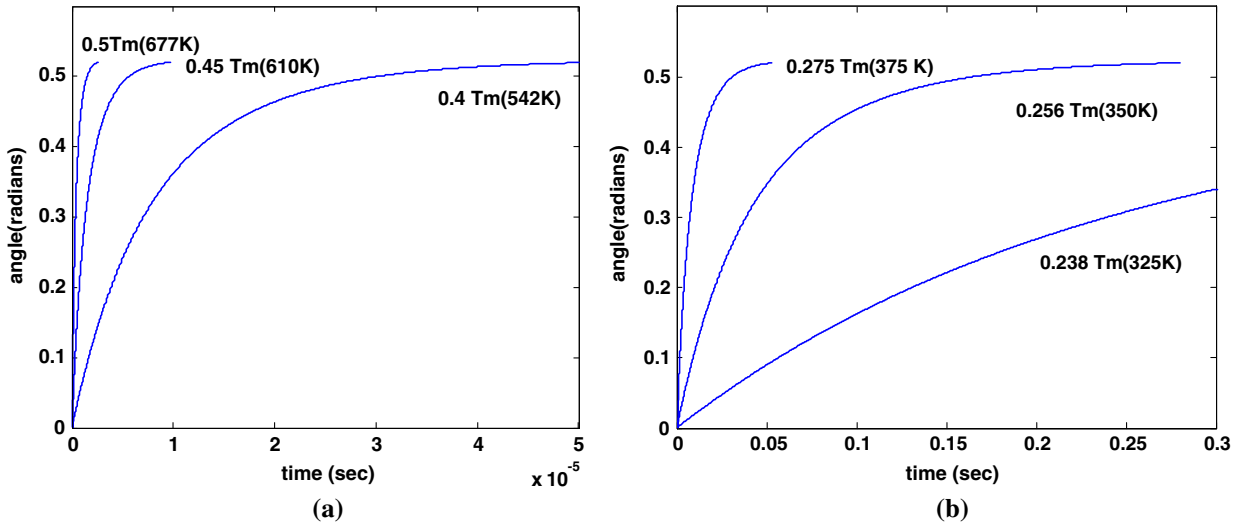

Fig. 27—Rotation angle as a function of time at different temperatures: (*a*) characteristic values in shear-band formation and (*b*) characteristic values for ECAP.

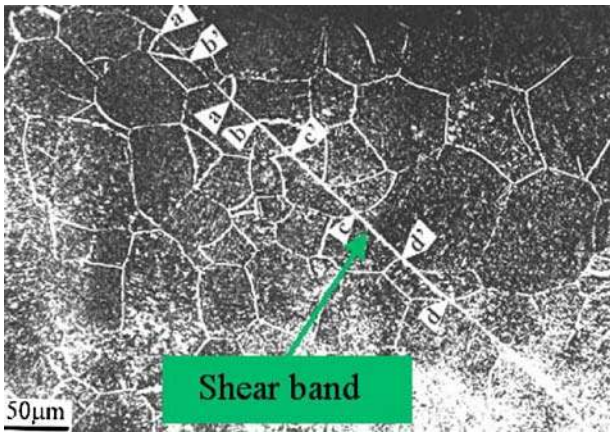

Fig. 28—Shear band in α-Ti developed during dynamic compression. Note: the grains on both sides of the band were sheared by shearing deformation, and made relative displacements.

α-Ti, as shown in Figure 28, where one can see that both sides of the band were displaced; for example, the displacements from a to a′, b to b′, c to c′, and d to d′ occur during localization. From these, it is found that the width of the shear band is 12 μm, and the average shear strain, which is the displacement divided by the width of the bands, was measured to be 5.2. According to the equation of the half-width of the shear band proposed by Dodd and Bai:[202]

$$\delta = \sqrt{\frac{\lambda\theta_*}{\tau_*\dot{\gamma}_*}} \qquad [7]$$

and the temperature rise within the bands was obtained by assuming that 90 pct of deformation work is converted into heat:

$$\theta_* = \frac{0.9\tau_*\gamma_*}{\rho \cdot c} \qquad [8]$$

The time required for shear-band formation can be obtained by the following equation from Eq. [7] with Eq. [8]:

$$t = \gamma_*/\dot{\gamma}_* = \frac{\rho c}{0.9\lambda}\delta^2 \qquad [9]$$

where $\tau_*, \dot{\gamma}_*$, are the shear stress and strain rate, θ_* is the temperature rise in the band, λ is the coefficient of the heat conduction, ρ is the material density, and c is the heat capacity. The parameters used in Eq. [3] are as follows: $\rho = 4.5$ g·cm^{-3}, $c = 0.473$ J g^{-1} K^{-1}, $\lambda = 14.63$ w m^{-1} K^{-1} for α-Ti, and $t = 0.1616\ \delta^2$, where the unit of the t is microsecond, and the unit of the δ is micrometer.

Grady[220] has another equation, of the form

$$\delta = \left(\frac{9\rho^3 C^2 \lambda^3}{\tau\alpha^2\dot{\gamma}}\right)^{1/4} \qquad [10]$$

where α is the thermal softening rate, assuming linear behavior ($\tau = \tau_0\ (1-\alpha T)$); the other parameters were previously defined. Grady later proposed another equation, in which the term 9 is replaced by 16.

From Eq. [9], it is found that the time required for formation of the band is 5.8 μs and, therefore, the strain rate that the shear band underwent is 9×10^5 s^{-1}, which is higher by two orders of magnitude than the average strain rate (2×10^3 s^{-1}) required for formation of the shear band, implying that formation of the shear band may accompany an abrupt increase in strain rate. In other words, the materials within the band underwent a super-high-strain-rate deformation. This is confirmed by the investigation of the Al-Li alloy.[77] Giovanola[103] measured directly the shear strain rate in the shear band as a function of time in VAR 4340 steel by using a high-speed photography technique, and found that shear localization occurs in two sequential stages: during the first localization, the strain rate (10^4 s^{-1}) jumps by more than an order of magnitude, then approaches 1.4×10^6 s^{-1} during the second localization. Such high strains and strain rates produced during localization in the bands have also been reported previously.[169]

A number of investigations show that a polycrystalline material with high-strain-rate sensitivity will appear to deform by a mode of superplastic flow.[169,204] First, the structures in the shear bands are very fine. Second, the temperature in the bands may reach and even exceed 0.4 T_m (T_m is the melting temperature). These provide the conditions for superplastic deformation of the materials in the bands. Ashby and Verrall[205] have proposed a constitutive equation to describe the superplastic flow of a material under high strain rate. They suggested that, when polycrystalline matter is deformed at a temperature above 0.4 T_m, one possible mode of superplastic flow is a "diffusion-accommodated flow." Dodd and Bai[202] have pointed out that, in the process of machining, although the average strain rate may be quite low, the strain rate in these narrow bands of shear may be markedly higher. Murr *et al.*[206] have also suggested that the shearing deformation actually achieved inside an adiabatic shear band is extremely large, with shear strains as large as 10, and that the mechanism by which this large strain is achieved involves DRX and superplastic flow by the sliding of submicron, equiaxed recrystallized grains. Indeed, it has been proposed that the extensive plastic deformation undergone by shaped charges is connected to the nanocrystalline grain structure generated by the deformation of the liner.[221]

J. *Dislocation Structure within the Bands*

Because the shear bands are so thin (micrometers or fractions thereof in width), it is usually difficult to prepare the specimens allowing the direct observation of the microstructure by TEM. Therefore, the information concerning these microstructure modifications obtained by TEM is scarce,[210] and the information reported is also conflicting.[211] The effects of shock on microstructure are well known and have been documented by Murr,[207] among others. Lee *et al.*[212] have investigated the microstructure within the shear band of HY-100 steel subjected to torsional loading using TEM, and

found that the center of the bands contains a mixture of the highly elongated narrow subgrains and fine equiaxed cells with a high dislocation density, and that the misorientations of 80 pct of the random cells have the angles of less than approximately 5 deg. They proposed that the primary metallurgical process occurring in the bands is dynamic recovery, resulting in both highly elongated subgrains and more equiaxed cellular structures. Meyers and Andrade *et al.*[213] have found that, as the band in the deformed specimen is approached, the equiaxed cells are replaced by elongated cells, and that these elongated cells inside the band break down and are replaced by small grains with a relatively low dislocation density. Therefore, they have attributed this kind of microstructure observed in TEM to DRX. Figure 29 is a typical example of a TEM structure; the details are taken from a region within the band in the low-carbon steel with the structure of the ferrite-cementite. Several characteristics are noteworthy. First, the α-ferrite in the band formed a tangled structure and the dislocation cells. The elongation and arrangement of the cells tend to be aligned along the shear direction, and the cell walls are full of dense dislocations, as shown in Figure 29(a). Second, the interfaces between the ferrite and cementite, as the sources, could form dislocations, as shown in Figure 29(b); the diffraction contrast analysis indicates that the majority of dislocations are single dislocations with Burgers vector 1/2[111] lying on a plane $(1\bar{1}0)$ and 1/2[$[1\bar{1}\bar{1}]$ lying on a plane (110). These dislocations may interact with each other to form a stable dislocation network (Figure 29(c)) expressed by: 1/2[111] + 1/2 $[1\bar{1}\bar{1}] \rightarrow [100]$. It might be expected that the formation of the tangles, cells, and networks of the dislocations could be responsible for the work hardening of the material in the shear bands during dynamic deformation. Third, the avalanche of the dislocation cells in the bands is observed in a specimen that is deformed to the point of failure, as shown in Figure 29(d). This may be proposed to be associated with the sharp drop of the load in the τ-γ response curve. Fourth, the strain distribution is heterogeneous from place to place along the shear band. This can be seen clearly in Figure 30, from the comparison of the SADPs from the different regions in the bands in a quenched steel. A relatively simple pattern is obtained from the region A (marked by circle A), implying that the crystallographic nature of this area in the shear band can be explained by slip deformation. On the other hand, in region C (marked by circle C), it shows a spotty ring pattern, indicating that the operation of multislip systems, arising from different subgrains with different suborientations in the area. All these show that strain distribution in the shear bands is heterogeneous, because of the inhomogeneous structures at microscale. The TEM examinations within the bands reveal the shear bands are highly localized regions that may cross through many grains. This implies that the shear bands are due to crystallographic slip on a governing slip system within one grain and penetrate into adjacent grains by cooperative slip events that may involve a number of slip systems. This kind of cooperative slip may be assisted by the stress concentrations at the grain boundaries. One of the interesting problems of the localized shear band is how the shear deformation develops from the microscopic bands in a grain into macroscopic bands on a spatial distribution, when it crosses the grain boundaries. Figure 31 shows a microscopic localized shear band crossing several grains with different orientations in a low-carbon steel. The trace of the band in grain C has a $\langle 111 \rangle$ direction, which coincides with the direction of the intersection of the thin-foil plane $(1\bar{4}1)$ with the slip plane $(11\bar{1})$ in grain B, suggesting that the shear deformation passes through the grain boundary by multi- or cross-slip systems. Electron contrast analysis shows that the grain C (marked by circle C), however, has the same trace as the grain B (marked by circle B), implying that the localized shear band propagates across the grain boundaries from one grain to the adjacent grain by single-slip systems.

Figure 32 shows a montage with the shear-band front in titanium. It can be seen that the tip varies in thickness from grain to grain, and that there is some

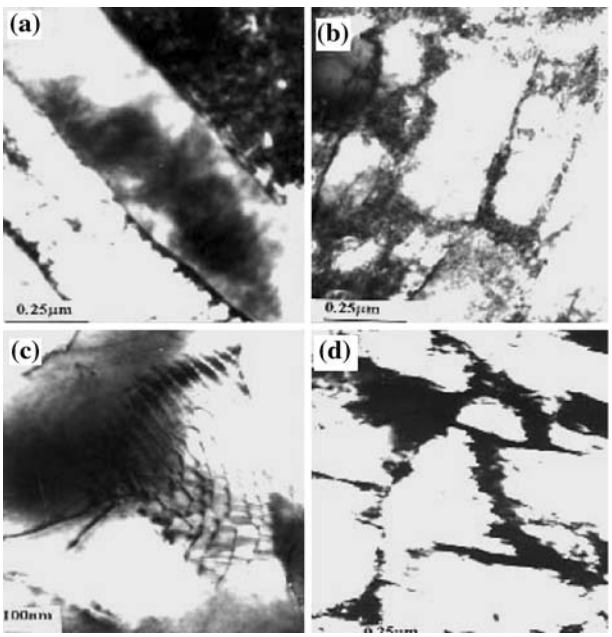

Fig. 29—A set of the TEM montage, showing the dislocation structure in the low-carbon steel subjected to dynamic torsional loading: elongated dislocation cells along the shear band and high dislocation density at the (*a*) and (*b*) cell walls, (*c*) hexagonal dislocation network, and (*d*) avalanche of the cells.

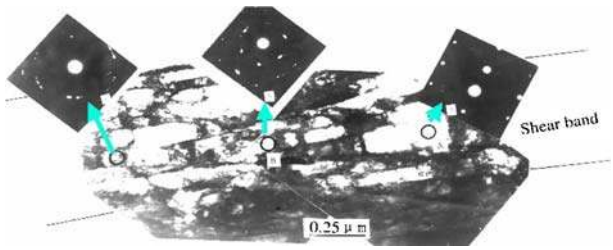

Fig. 30—Microstructure within the shear band generated during dynamic torsional loading in low-carbon steel.

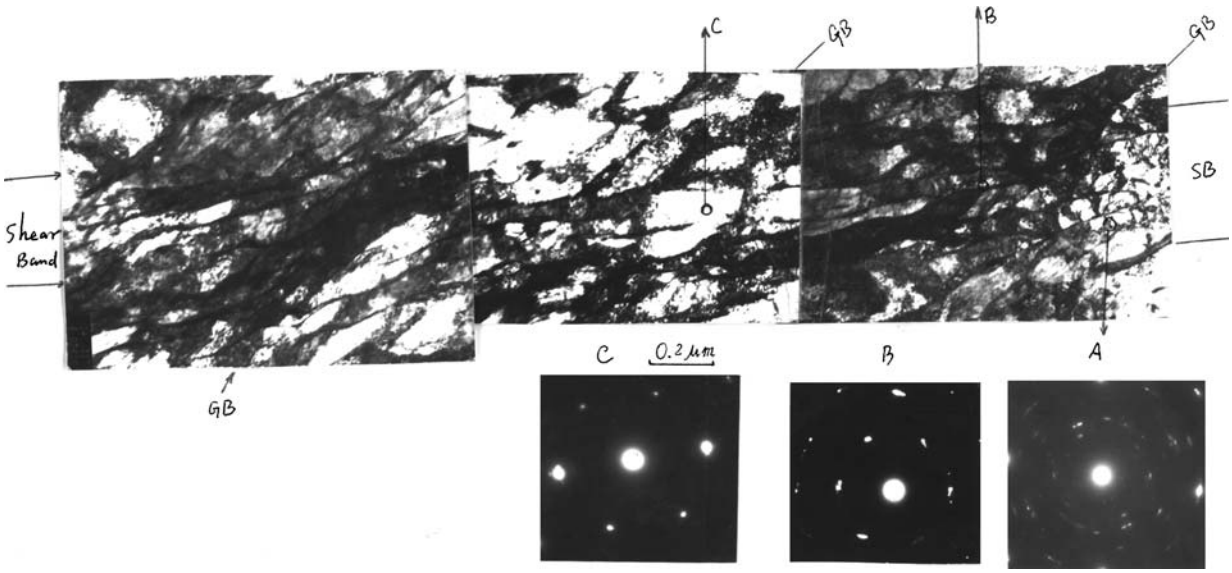

Fig. 31—Montage of TEM micrographs, showing microscopic shear band crossing several grains by different slip modes at grain boundaries in a low-carbon steel.

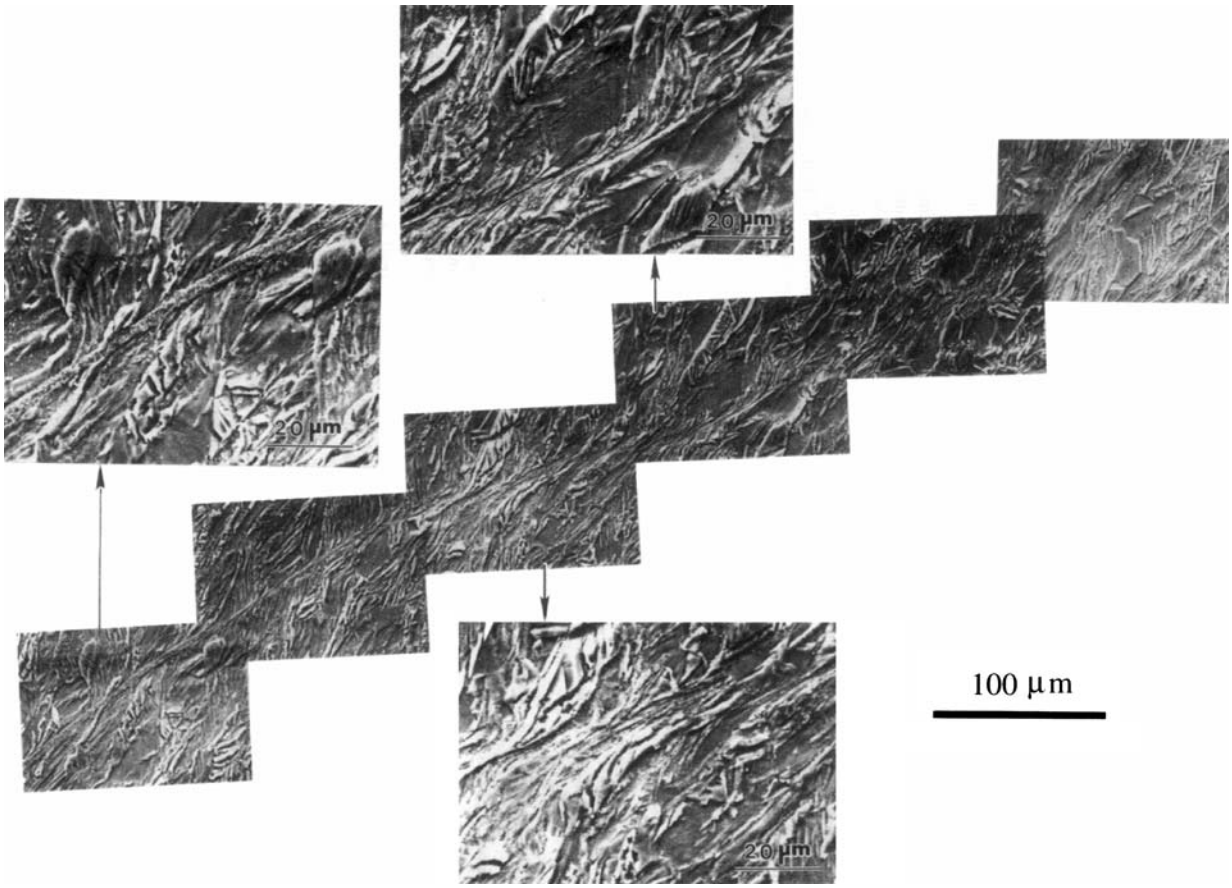

Fig. 32—Shear-band front in titanium; pictures on sides are higher magnifications.

''meandering'' before the shear band is clearly defined. Larger magnification pictures are seen on the sides of the main band to reveal the details of the propagating front. The shear-band thickness as well as the intensity of localization vary from grain to grain. This is definitely initiated by crystallographic slip on a few grains and subsequently defines itself,[81] as these regions of deformation connect.

K. *Damage and Fracture along the Shear Bands*

The interrupted tests mentioned in Section II show that the sudden drop appearing in the τ-γ curve, leading to fracture, is caused by the initiation and coalescence of the microcracks along the bands, rather than by the formation of the shear bands. The localized shear deformation promotes further nucleation, growth, and coalescence of the microcracks and, therefore, accelerates the fracture of material along the bands. The degree of structural damage in the shear bands leading to final failure along the bands can be assessed as shown in Figure 33. The number of cracks per square millimeter, which is an indication of the degree of the structural damage, was determined as a function of the distance from the boundary between the shear bands and matrix to the center of the band of the dual-phase steel subjected to dynamic torsional loading. It can seen that the nearer the center of the band, the bigger the structural damage extent. The final break is obvious along the shear band, as shown in Figures 34 and 35, which indicate the fracture along the bands of Al-Li alloy (Figure 34) and Al/SiC_p composite (Figure 35), respectively. These observations are in good agreement with the results obtained by Hartley *et al.*[40] Concerning the fracture of the materials subjected to dynamic loading under a high strain rate, detailed discussions were given by Rogers,[21] Meyers,[27] and Brandon;[214] they classified the fracture induced during high-strain-rate loading as either ductile or brittle in nature. Rogers reported[21] that if the fracture is ductile, it almost certainly occurred during adiabatic deformation, when the band was hot and weak. On the other hand, brittle fracture, which is particularly common in transformed bands in steels, occurs subsequent to the termination of deformation and the quenching of the hot band by the adiabatic matrix material to form the hard, brittle, transformed structure. However, a number of observations of the fracture surface by SEM reveal that, whether the fracture occurs along the deformed type bands in quenched martensite steels[44] or the white-shear bands in Ti-55 alloys[215] and Al-Li alloys,[77] their fracture topographies appeared to be of ductility characterized by the shear dimples on the fracture surface, as demonstrated in Figure 36. Guduru *et al.*[141] similarly obtained the classic inclined dimple pattern in a fractured shear band in maraging steel, confirming that the fracture is ductile and occurs inside of the band while it is at a high temperature.

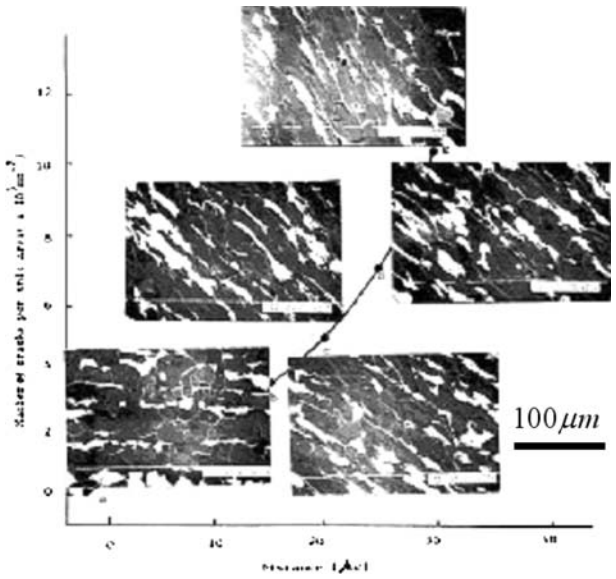

Fig. 33—The relationship between the number of the cracks per square millimeter and the distance from the boundary of the band to the matrix in the shear band, in low-carbon steel.

Fig. 34—Fracturing along the shear bands in Al-Li alloy subjected to dynamic impact compression.

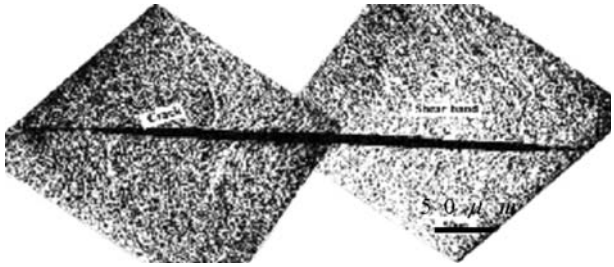

Fig. 35—Fracturing along the shear bands in Al/SiC_p composite alloy subjected to dynamic impact compression.

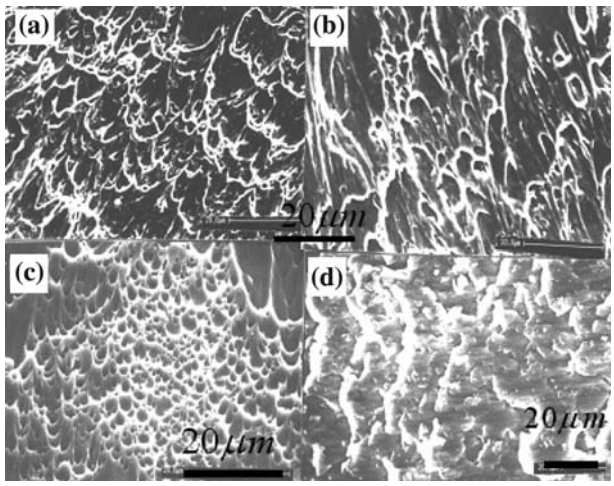

Fig. 36—Fracture surface morphologies observed in the deformed bands in Ti-6Al-4V alloy: (*a*) quenched-martensite steel, (*b*) in the white-etching bands in Al-Li alloy and (*c*) titanium alloy, and (*d*) subjected to dynamic loading under high strain rate.

It is known that the fracture surface morphology of the quenched steel should be cleavage or quasi-cleavage.[216] However, there are no cleaved faces or other brittle features to be observed on the fracture surface in this steel, particularly in the case of the quenched steels. The materials in the bands subjected to a large accumulated strain under a high strain rate, resulting in a temperature rise, seem to suffer an annealing or temper treatment, leading to structural softening. Therefore, the fracture morphology in the quenched steel deformed at a high strain rate and large strain appears to be similar to those in the annealed or tempered steels; thus, it is reasonable to propose that, in addition to the stress state condition, the temperature rise within the band plays an important role in the failure of materials along the shear bands, as mentioned by Rogers.[21] The temperature rise in the shear band is so high that it can cause recrystallization or even melting, leading to softening of the material in comparison with that in the adjacent matrix. Timothy and Hutchings assumed[34] that the void formation in adiabatic shear bands in titanium alloys was intimately associated with the thermal softening and local melting of the metal in the shear bands. So, this is the reason that, in all cases, the fracture surface topography observed is entirely of a ductile nature, irrespective of whether it is occurring in the deformed or white-etching shear bands in quenched and tempered steels.

Figure 37 shows voids that nucleated and grew inside the shear bands in Ti-6Al-4V. If, subsequent to void nucleation, there is some tension, these voids grow until their edges reach the boundary of the shear band. Then they do not grow into the surrounding material, because of its higher yield strength. The voids become gradually ellipsoidal, as they elongate along the shear bands. This sequence is shown in Figure 37(b). As they grow, they eventually coalesce, forming a crack.

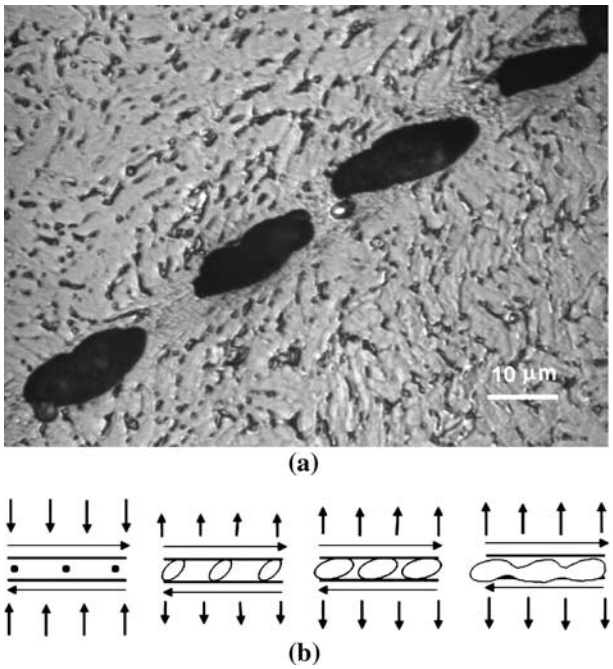

Fig. 37—(*a*) Ductile fracture inside shear band in Ti and (*b*) schematic representation of sequence of events leading to ductile failure.

Zhou *et al.*[218] measured the velocity of propagation of shear bands in a Ti6Al4V alloy impacted at a velocity of 50 m/s. Their propagation velocities were 50 to 75 m/s. Xue *et al.*[217] used the TWC method, which had an initial wall velocity of 200 m/s and obtained a propagation velocity of 556 m/s, inferred from their experimental results. This great difference can be explained through Mercier and Molinari's[219] analysis: the imposed velocity C determines the shear-band velocity V through the equation

$$V = \frac{\sigma_f}{\rho C} g\left(\frac{\lambda}{h}\frac{t}{h}\right) \qquad [11]$$

where σ_f is the material flow stress and g is a function of λ/h, the normalized process zone length, and t/h, the normalized shear-band thickness. Figure 38 shows the effect of flow stress on the velocity of propagation of the shear band. Two experimental points are given: one for Ti and one for Ti6Al4V, with a flow stress approximately triple the one for pure Ti. There is a linear relationship between flow stress and V, for the same external conditions and g. The experimental results by Xue *et al.*[217] compare well with the Mercier–Molinari predictions.

L. *Spacing and Self-Organization of Shear Bands*

Collective organization processes take place during the formation of shear bands. Most of the current theories on prediction of spacing of shear bands are based on the analysis of a single shear band along its propagating direction. The theories by Grady and Kipp,[86] Wright and Ockendon,[88] and Molinari[89] are presented in the companion paper in these proceedings by Walley.[224] The three equations are given in Table III. We describe briefly below the evolution of multiple adiabatic shear bands in commercially pure titanium and Ti-6Al-4V alloy through the radial collapse technique of a thick-walled cylinder under high-strain-rate deformation (experimental configuration

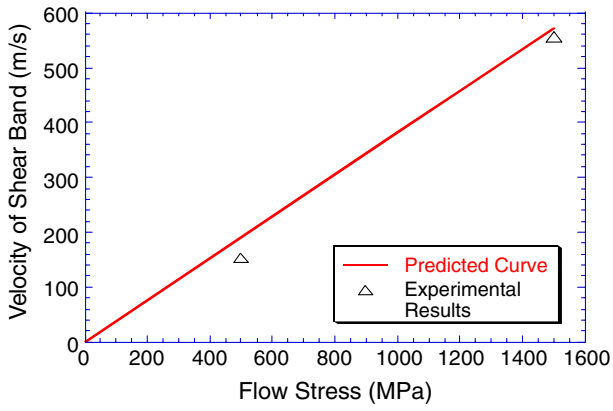

Fig. 38—Shear-band velocity as a function of flow stress for Ti alloys; comparison of Mercier–Molinari theory[219] with results by Xue *et al.*[39]

Table III. Comparison of Theoretical Predictions for Shear Band Spacing Without Strain Hardening

Prediction	Grady–Kipp Model	Wright–Ockendon Model	Molinari Model
Spacing	$2\pi\left[\frac{kC}{\dot{\gamma}_0^3 a^2 \tau_0}\right]^{1/4} \cdot \frac{9^{1/4}}{\pi}$	$2\pi\left[\frac{kC}{\dot{\gamma}_0^3 a^2 \tau_0}\right]^{1/4} \cdot m^{3/4}$	$2\pi\left[\frac{kC}{\dot{\gamma}_0^3 \tau_0 a^2}\right]^{1/4} \cdot \left[\frac{m^3(1-aT_0)^2}{(1+m)}\right]^{1/4}$

shown in Figure 1(c). Shear-band initiation, propagation, as well as spatial distribution were examined under increasing global strains. As an illustration, Figure 39(a) shows the pattern of helicoidal shear bands in a Ti-6Al-4V specimen, whereas Figure 39(b) shows the size and spatial distribution of these bands at a global effective strain of 0.264. The shear bands nucleate at the internal boundary of the specimens and construct a periodical distribution at an early stage. The shear bands undergo bifurcation as they progress in their spiral trajectory and as their spacing increases. The shear bands are favored initiation sites for failure, which occurs by void nucleation, growth, and coalescence inside the thermally softened regions. The evolution of the morphology of the voids is determined by the restrictions imposed by the bands. Figure 40 shows that the shear-band spacing is quite dependent on the material, being much lower in 304 stainless steel than in the Ti-6Al-4 V. The differences of mechanical response between the two alloys are responsible for significant differences in the evolution of the shear band patterns. The same differences are observed between titanium and Ti-6Al-4V. Figure 41 shows how the shear-band spacing and its evolution determines the fragmentation of a cylindrical specimen. The number of shear bands initiated in Ti (spacing

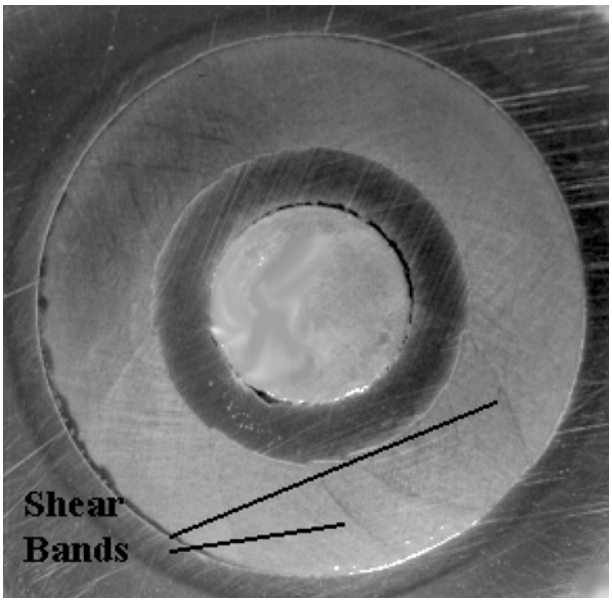

(a) Shear band pattern, N=68

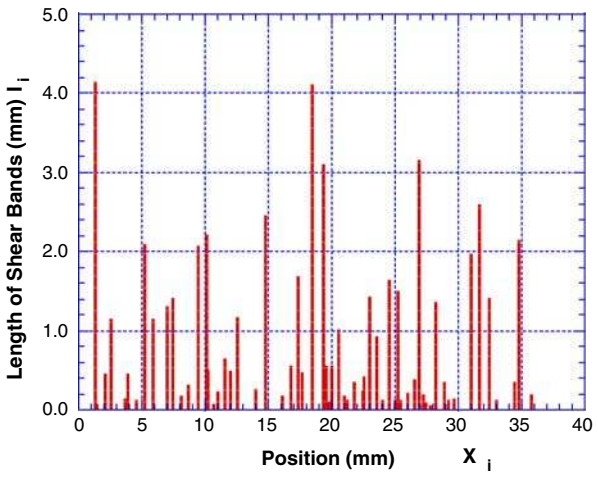

(b) Spatial distribution

Fig. 39—Shear-band pattern of Ti-6Al-4V alloy at well developed stage $\varepsilon_{eff} = 0.264$.

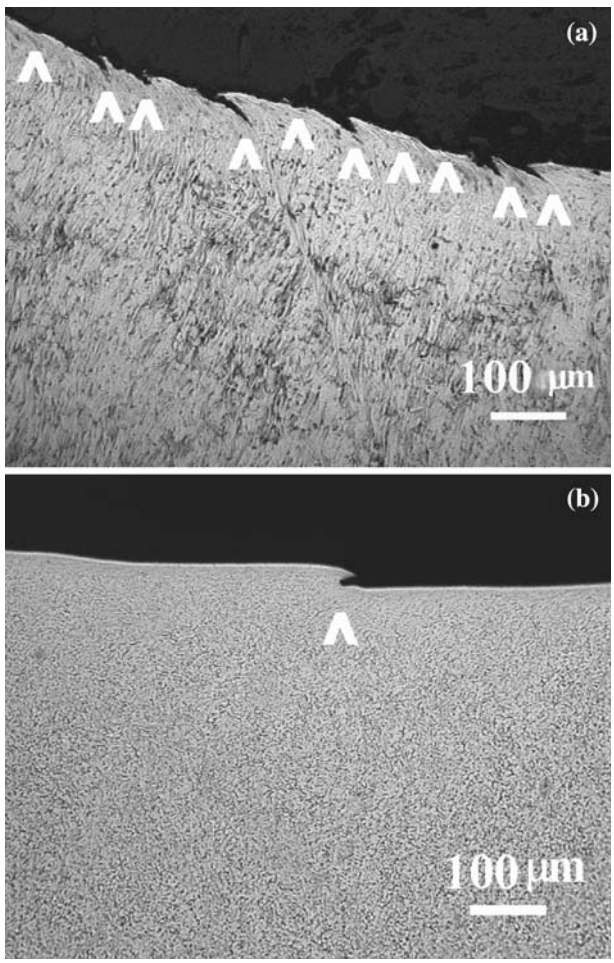

Fig. 40—Comparison of spacings for stainless steel (*a*) and Ti-6Al-4V alloy (*b*) at initial stage.

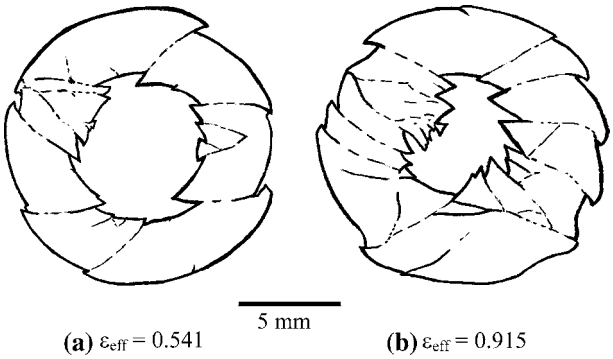

Fig. 41—Evolution of shear band pattern in Ti-6Al-4V alloy.

of 0.18 mm) is considerably larger than in Ti-6% Al-4%V (spacing of 0.53 mm). The experimentally obtained shear-band spacings are compared with theoretical predictions by Grady and Kipp,[86] Wright and Ockendon,[88] and Molinari[89] in Table IV. The shear-band interactions are more complex than previously thought and their spacing cannot be predicted by the one-dimensional perturbation theories of Wright and Ockendon[88] and Molinari.[89] The Grady–Kipp theory cannot accommodate the increased spacing as the shear-band size increases, since it is also one-dimensional. This was done by Xu *et al.*[61,62] Thus, the treatment needs to incorporate elements that are outlined below:

(a) Rate of nucleation of shear bands. The probability of nucleation, $p(v_0, s_0)$, in a reference volume v_0, or surface s_0 was successfully described by a Weibull distribution in which the stress was replaced by strain as the independent variable. Parameters defining the distribution are a critical strain for nucleation, a mean nucleation strain, and a Weibull modulus. There can also be shielding at the nucleation stage, depending on the relative values of the rate of nucleation and rate of growth.

(b) Rate of growth, or velocity of propagation. This is an important factor in their self organization. Shear bands compete among themselves and gradually change their patterns. A "Darwinian" natural selection takes place, and a large number of small bands evolve gradually into a smaller number of large bands, due to the shielding of stresses produced during growth. Such evolution of shear band pattern occurs under a homogeneously distributed pressure acting on the external boundary of the cylindrical specimen. This is a typical self-organization. This is schematically rendered in Figures 42 and 43.

This theory was developed by Xue *et al.*[61,62] and applied to Ti, Ti6Al4V, and 304 SS. It clearly needs additional work.

It is indeed interesting that shear-band spacing plays a role in deformation of metallic glasses. Indeed, Conner *et al.*[225] measured the spacing in quasistatic bending of a Zr based BMG and found it to be ~0.1 mm initially. Eventually a few shear bands grow and dominate the process as in the case of dynamic deformation.

IV. CONCLUSIONS

From the results presented in the previous sections, the following useful conclusions can be made:

1. The initiation of the shear localized band occurs with a crystallographic slip in a favored individual grain which then propagates into the adjacent

Table IV. Predictions and Experimental Results for Stainless Steel and Titanium

Spacing (mm)	Exp. Data Initial Level	Exp. Data Developed	L_{WO} (mm)	L_{GK} (mm)	L_{MO} (mm)
SS 304L	0.12	3.2	0.17	2.62	0.16
CP Titanium	0.69	2.57	0.52	3.3	0.36

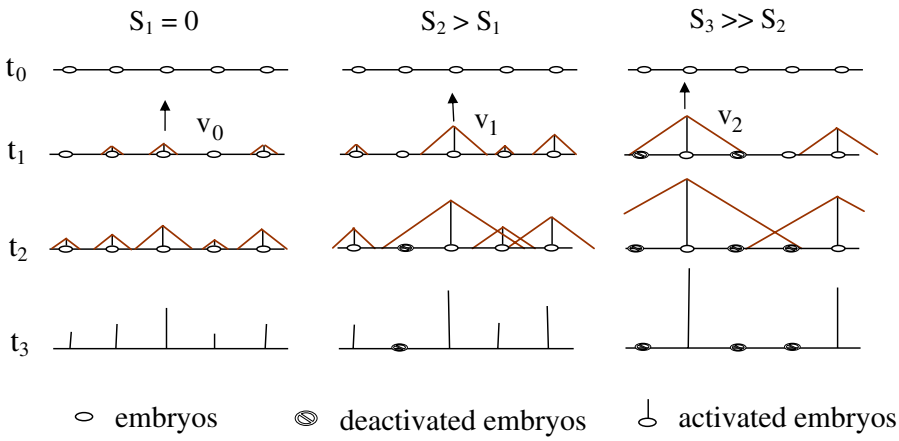

Fig. 42—Two-dimensional representation of concurrent nucleation and shielding. S is a shielding parameter; as S increases, the release of stress produced by growing shear band deactivates embryos. For S = 0, all embryos are activated and shear-band spacing is small. For large value of shielding S_3, (right hand side) only a fraction of embryos are activated.

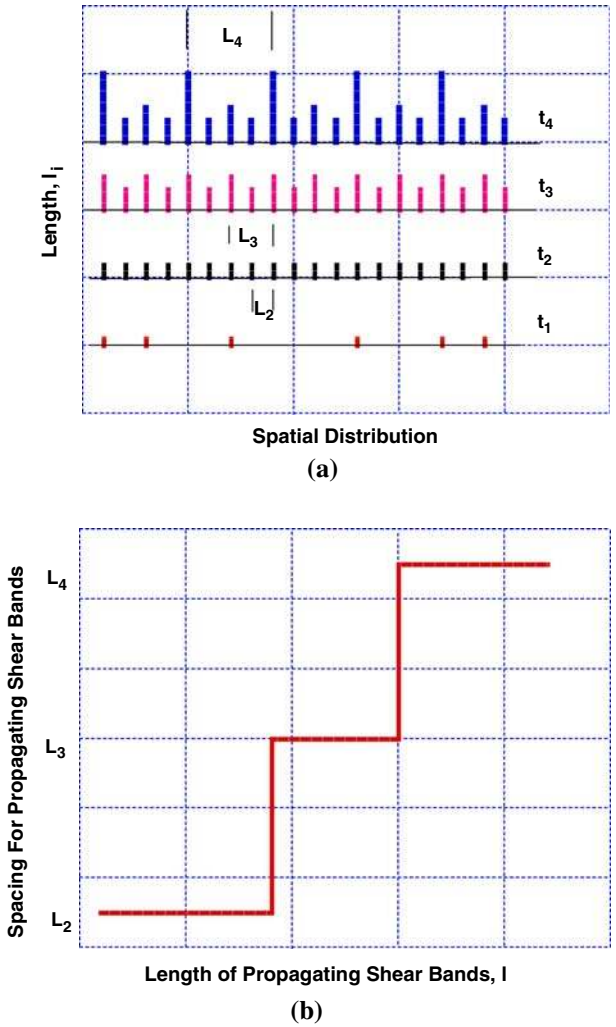

Fig. 43—(*a*) Schematic diagram of the evolution of shear band spacing at different levels. t_1-Random initiation; t_2-self organization into "periodic" pattern among nuclei; t_3-some shear bands grow faster suppressing others; t_4-self organization of developed shear bands. (*b*) Spacing of propagating SBs as a function of length.

grains by cooperative slip or cross-slip, leading to spread of shear localization over the total cross-section of the deformed specimen, eventually propagating to a macroscopic shear band.

2. There is a critical shear strain required for shear-band formation at a specific strain rate. In other words, in addition to a critical strain, a critical strain rate is also required for the formation of the shear band. This is supported by the experimental results Ti and Al-Li alloys.
3. Deformed and 'transformed' shear bands are proposed to form at different deformation stages during localization. The deformed bands form first. 'Transformed' bands have a white etching coloration in optical microscopy, most probably due to the small scale of the grain structure generated. It is proposed that 'transformed' bands indeed the result of recrystallization in the structure.
4. Phase transformations have been observed in the shear bands in Ti-6Al-4V alloy and 304 stainless steel as well as Fe-Ni-Cr monocrystals during explosive collapsed testing, and the phase transformation products have a certain crystallographic orientation relationship with their parent matrix.
5. The sharp drop in the load-carrying capability on the shear stress-strain response for the deformed specimen seems to be closely associated with a certain critical coalescence of the microcracks or voids in the bands, rather than the occurrence of the shear bands per se.
6. The shear deformation localization process involves sequential conventional crystallographic and non-crystallographic deformation events within the band, including slip and twinning in individual grains, cooperative slip and cross-slip at grain boundaries, strain and strain rate-hardening (dislocation reactions, cell formation, substructure generation). Added to these are special mechanisms: softening arising from the rise of temperature in the band, breakup of the deformation structure through rotational dynamic recrystallization, structural damage resulting from the initiation, growth and coalescence of the cracks or voids, and finally, the fracture along the shear bands. Figure 44 shows, in a schematic fashion, the phenomena taking place as a shear band forms. At the front, we have intermittent slip/twinning dependent on the grain orientation. These intermittent slip regions gradually join up and form a deformation band which traverses grain boundaries. As the displacement increases (farther from front) the deformation band reorganizes itself into an ultrafine grained/recrystallized structure.
7. The current observations in copper, tantalum, brass, stainless steel, Al-Li alloy, Ti and Ti-alloys, IF steel, and Zircaloy show that recrystallization often occurs in the shear bands, beyond a critical strain. The widespread evidence of the equiaxed and distortion-free grains (obtained through TEM observations) can be reasonably explained by a rotational dynamic recrystallization mechanism that may or not be followed by static grain growth, depending on the post deformation cooling.
8. The microstructures observed in adiabatic shear bands (sub micrometer equiaxed grains) are similar the one in metals processed by severe plastic

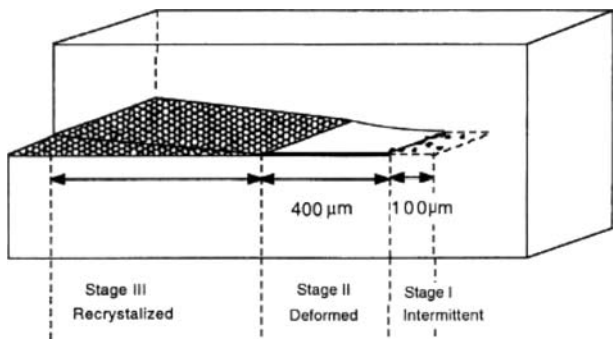

Fig. 44—Schematic representation of shear-band front in T_i showing three regions: intermittent slip at grain scale, deformed region, and recrystallized/ultrafine-grained region.

deformation (SPD) methods. Therefore, it is proposed that the grain refinement mechanism may be the same.

9. The shear bands self organize with a spacing that is a function of the mechanical and thermal response of the material as well as external imposed conditions (stress state, strain rate, pressure, etc). This spacing has been compared with predictions by Grady and Kipp,[86] Wright and Ockendon,[88] and Molinari.[89] The two-dimensional nature of the process is such that the characteristic spacing changed with shear-band length. This was treated by Xue *et al.*[61,62]

In summary, we present results of individual and collaborative investigations on the microstructural aspects of shear localization in materials under high strain rates and also review and discuss some important phenomena such as phase transformations, dynamic recrystallization leading the structure from polycrystalline to nanocrystalline, possible amorphous, super-high strain rate deformation within the band, and the evolution process of shear localization.

V. RECOMMENDED AREAS FOR FURTHER INVESTIGATION

The study of shear bands, entering its seventh decade, will still yield original and novel results, since a number of the scientific questions have not been satisfactorily answered to this day. We indicate below some of the areas that would be worthwhile of scientific inquiry. The overview by Rosakis and Ravichandran[228] on this complements the recommendations below.

1. Advanced sample preparation and characterization tools will significantly accelerate our understanding of shear bands. As we mentioned earlier, there is difficulty in preparing the samples for TEM and X-ray examination, and therefore the information from TEM and X-ray examination presented here is still limited. For a better understanding of the shear banding, the measurement and systematic observations of the microstructures need to be pursued further. The focused ion beam (FIB) technique can play an important role in this endeavor.
2. Shear localization under quasistatic and dynamic loading conditions in bulk metallic glasses. Is the shear band propagation a dynamic event even if loading is static? The release of the elastic energy stored in system is, in this case, the driving energy. There are two views on the softening mechanism leading to localization: thermal softening, observed by Lewandowski and Greer[3] and free volume coalescence softening, proposed by Spaepen.[232] Dai *et al.*[233] and Liu *et al.*[234] performed experiments and calculations that indicate that both mechanisms are operative in the $Zr_{41.2}Ti_{13.8}Cu_{12.5}Be_{22.5}$ bulk metallic glasses.
3. The Nix freezup hypothesis: Nix[230] observed that the shear bands in metallic glasses loaded quasistatically propagate a certain distance and then stop. Figure 45 shows a sequence of events. A shear band initiates at the surface of specimen (Figure 45(b)), and propagates at a velocity V_1. The thermally softened region has a length a_1. As the band propagates down (Figure 45(c)), the region away from the band cools down and can 'freeze' back. This reduces the driving energy for the band and reduces the length of the softened region to a_2. Thus, one would expect an associated reduction in propagation velocity to V_2. This velocity is reduced to zero in Figure 45(d), when the softened region length reaches a critical size a_3.
4. Real-time experimental examination of the two-dimensional deformation in propagating shear bands: This has two components:
   (a) Propagation velocity as a function of applied stress. The experiments developed by Zhou, Ravichandran and Rosakis[218] reveal an extremely important characteristic of shear bands: their propagation velocity. More systematic experimentation is needed to understand how the velocity is related to the constitutive response in metals and alloys. Is it possible to develop a generalized theory? Is the Mercier-Molinari[219] theory applicable over a broad spectrum?
   (b) The temperature rise plays a key role in the formation of the shear bands, but has not been determined precisely at present.
5. Shear band propagation in multiaxial loading. The experiments described herein use three techniques

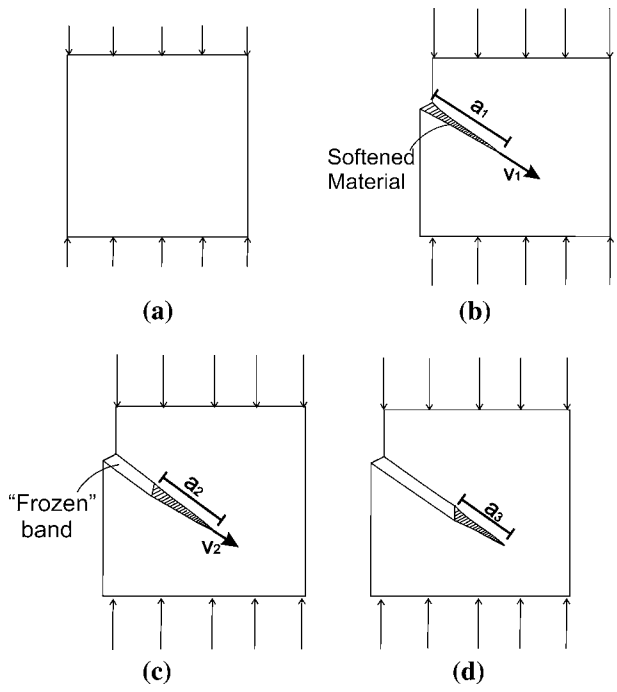

Fig. 45—Schematic sequence showing how a shear band initiates, propagates, and arrests in a bulk metallic glass subjected to quasistatic compression.

providing three stress states. Nevertheless, there was no attempt to systematically vary the stress state. This area needs systematic investigation. Experimental results by Meyer[231] indicate that small variations in stress state have a significant effect on the initiation strain for localization. The effect of hydrostatic stresses needs to be established, since shear bands grow during high pressure dynamic events.

6. Thermal softening at high rates. The microstructural changes that are well documented undoubtedly affect the thermal softening. However, the exact nature of this softening is virtually unknown. As shown by Eq. [10] (linearized assumption), the thickness and spacing of bands (Table III) are directly dependent on this softening. The constitutive approach by Molinari and Ravichandran[227] might be a good effort in that direction.
7. Amorphization within shear bands. The preliminary report by Meyers *et al.*[63] needs to be confirmed.
8. A better understanding of the rate sensitivity of work hardening is needed for improved constitutive description. The Los Alamos MTS model pioneered by Kocks and coworkers[226] incorporates this effect through a dislocation evolution term, but the physical basis needs experimental verification.
9. The ultrafine grain size within the shear bands: what are the contributions of rotational recrystallization, post-deformation recrystallization and grain growth processes on the recovered microstructure?
10. Although this review has focused primarily on single localized shear band, in many cases, multibands, and even large and complex network of bands occur. The self-organization of bands is a new topic of study requiring both experimental and theoretical investigations. Further experimental investigation is needed in order to provide the modeling of such complicated behavior.
11. Many alloys (steels, titanium and aluminum alloys) that undergo dynamic strain aging are also prone to shear localization.[229] What is the effect of the changes in thermal softening and strain-rate sensitivity on the development of shear bands?
12. Both shear-band bifurcation and the development of a quantitative treatment of a shear band toughness (initially proposed by Grady[220]) are desirable and necessary areas of research.

Finally, although there is rather good relation between theoretical analyses and experimental results, the experimental data that can be directly compared with these analyses to verify and guide model development of shear localization are still scarce. Materials researchers need to provide clear descriptions of the nano/micro/mesostructural evolution, thus enabling Mechanicians performing theoretical analyses to arrive at more complete constitutive descriptions. Mechanics and Materials researchers should come together more often to accelerate the understanding of the phenomena.

ACKNOWLEDGMENTS

This research supported by the National Natural Science Foundation of China Grant No. 50071064, 19891180-2 and 19392300; by The Chinese Academy of Sciences under Special Grant 87-52: by the US Army Research Office MURI programs at UCSD in the 1988-1998 period; by the US National Science Foundation Division of Engineering (Institute for Mechanics and Materials). Collaborations and discussions with former students and colleagues, Drs. Z.C. Li, T.W. Wright, W.L. Zhong, J.Q. Yu, Y.J. Chen, Q. Xue, J.C. La Salvia, X.L. Huang, G.T. Gray, D. Kong, H. Li, Q. Xue, E. Cerreta, B. Kad, M. Ehlers, U.R. Andrade, J.H. Beatty, T. Perez-Prado, L. Wittman, Profs. V.F. Nesterenko, L.W. Meyer, K.S. Vecchio, Q. Li, T. Shen, Z. Ling, J.H. Zhang, G. Subhash, and Z.G. Wang are greatly appreciated. Professor G. Ravichandran generously contributed to the last section on suggested areas for future research and shared his wisdom with the authors. Especially, Dr. W.L. Zhong, Dr. J.Q. Yu, Dr. Z.C. Li, Dr. E. Cerreta, Dr. B. Kad, and Profs. Q. Li and K.S. Vecchio have joined this joint program and provided a number of micrographs and experimental data for this paper. Their contributions to this project are gratefully acknowledged. The photographs were taken by TEM and HREM in the State Key Laboratory of Fatigue and Fracture for Materials, Atomic Image Laboratory of the Chinese Academy of Sciences, Oak Ridge National Laboratory, and UCSD Electron Microscopy Center.

REFERENCES

1. C. Zener and J.H. Hollomon: *J. Appl. Phys.*, 1944, vol. 15, p. 22.
2. H. Tresca: *Proc. Inst. Mech. Eng.*, 1878, vol. 30, pp. 301–45.
3. J.J. Lewandowski and A.L. Greer: *Nat. Mater.*, 2006, vol. 5, pp. 15–18.
4. D. Jia, K.T. Ramesh, and E. Ma: *Acta Mater.*, 2003, vol. 51, pp. 3495–3509.
5. Q. Wei, L. Kecskes, T. Liao, K.T. Hartwig, K.T. Ramesh, and E. Ma: *Acta Mater.*, 2004, vol. 52, pp. 1859–69.
6. R.F. Recht: *J. Appl. Mech.*, 1964, vol. 31, p. 189.
7. R.S. Culver: in *Metallurgical Effects at High Strain Rates*, R.W. Rohde, B.M. Butcher, J.R. Holland, and C.H. Karnes, eds., Plenum Press, New York, NY, 1973, p. 519.
8. R.J. Clifton: *Material Response to Ultra-High Loading Rates*, Report NMAB-356, National Advisory Board Committee, Washington, DC, 1980, ch. 8.
9. Y.L. Bai: in *Shock-Waves and High-Strain-Rate Phenomena*, L.E. Murr and M.A. Meyers, eds., Plenum Press, New York, NY, 1981, p. 277.
10. T.J. Burns and T.G. Trucano: *Mech. Mater.*, 1982, vol. 1, p. 313.
11. J. Pan: *Int. J. Solid Struct.*, 1983, vol. 19, p. 153.
12. S.L. Semiatin, M.R. Staker, and J.J. Jonas: *Acta Metall.*, 1984, vol. 32, p. 1347.
13. F.H. Wu and L.B. Freund: *J. Mech. Phys. Solids*, 1984, vol. 32, p. 119.
14. T.W. Wright and R.C. Batra: *J. Phys.*, 1985, vol. C5 (45), p. 323.

15. C. Fressengeas and A. Molinari: *J. Mech. Phys. Solids*, 1987, vol. 35, p. 185.
16. J.R. Johnson: *J. Eng. Mater. Technol.*, 1981, vol. 103, p. 201.
17. D.A. Drew and J.E. Flaherty: in *Phase Transformation and Material Instabilities in Solids*, M.E. Gurtin, ed., Academic Press, Orlando, FL, 1984, p. 37.
18. J. Lemonds and A. Needleman: *Mech. Mater.*, 1986, vol. 5, p. 339.
19. V. Tvergaard: *J. Mech. Phys. Solids*, 1987, vol. 35, p. 43.
20. P.M. Anderson, N.A. Fleck, and K.L. Johnson: *J. Mech. Phys. Solids*, 1990, vol. 38, p. 681.
21. H.C. Rogers: *Annu. Rev. Mater. Sci.*, 1979, vol. 9, p. 283.
22. H.C. Rogers: in *Material Behavior under High Stress and Ultra High Loading Rates*, J. Mescall and V. Weiss, eds., Plenum Press, New York, NY, 1983, p. 101.
23. M Stelly and R. Dormeval: in *Metallurgical Applications of Shock Waves and High-Strain-Rate Phenomena*, L.E. Murr, K.P. Staudhammer and M.A. Meyers, eds., Marcel Dekker, New York, NY, 1986, p. 60.
24. S.P. Timothy: *Acta Mater.*, 1987, vol. 35, p. 301.
25. L.E. Murr: in *Materials at High Strain Rates*, T.Z. Blazynski, ed., Elsevier Applied Science Publishers, Essex, England, 1987, pp. 1–45.
26. R. Dormeval: in *Materials at High Strain Rates*, T.Z. Blazynski, ed., Elsevier Applied Science Publishers, Essex, England, 1987, p. 47.
27. M.A. Meyers: in *Mechanics and Materials—Fundamentals and Linkages*, M.A. Meyers, R.W. Armstrong, and H.O.K. Kirchner, eds., John Wiley, New York, 1999, p. 14.
28. M.A. Meyers: *Encyclopedia of Materials: Science and Technology*, Oxford, UK, 2001, pp. 7093–103.
29. H.A. Grebe, H.R. Park, and M.A. Meyers: *Metall. Trans. A*, 1985, vol. 16A, p. 761.
30. M. Stelly, J. Legrand, and R. Dormeval: in *Shock Waves and High-Strain-Rate Phenomena*, L.E. Murr and M.A. Meyers, eds., Plenum Press, New York, NY, 1981, p. 113.
31. A. Marchand and J. Duffy: *J. Mech. Phys. Solids*, 1988, vol. 36, p. 251.
32. D.A. Shockey, D.R. Curran, and P.S. De Carli: *J. Appl. Phys.*, 1975, vol. 46, p. 3766.
33. Y. Me-Bar and D. Shechtman: *Mater. Sci. Eng.*, 1983, vol. 58, p. 181.
34. S.P. Timothy and I.M. Hutchings: *Mater. Sci. Technol.*, 1985, vol. 1, p. 526.
35. M.A. Meyers and H.-R. Pak: *Acta Metall.*, 1986, vol. 34, p. 2493.
36. M.A. Meyers, G. Subhash, B.K. Kad, and L. Prasad: *Mech. Mater.*, 1994, vol. 17, p. 175.
37. M.G. da Silva and K.T. Ramesh: *Mater. Sci. Eng.*, 1997, vol. 232, p. 11.
38. D.R. Chichili, K.T. Ramesh, and K.J. Hempker: *Acta Mater.*, 1998, vol. 46, p. 1025.
39. Q. Xue, M.A. Meyers, and N.F. Nesterenko: *Acta Mater.*, 2002, vol. 50, p. 575.
40. K.A. Hartley, J. Duffy, and R.H. Hawley: *J. Mech. Phys. Solids*, 1987, vol. 35, p. 283.
41. Y.L. Bai, Q. Xue, and Y.B. Xu: *Mech. Mater.*, 1994, vol. 17, p. 155.
42. Y.L. Bai, Q. Xue, Y.B. Xu, and L.T. Shen: in *Metallurgical and Materials Application of Shock Waves and High-Strain-Rate Phenomena*, L.E. Murr, K.P. Staudhammer, and M.A. Meyers, eds., Elsevier Science, Amsterdam, 1995, p. 385.
43. Y.J. Chen, M.A. Meyers, and V.F. Nesterengo: *Mater. Sci. Eng.*, 1999, vol. A268, p. 70.
44. Y.B. Xu, Y.L. Bai, and L.T. Shen: *Acta Metall.*, 1996, vol. 44, p. 1917.
45. S.A. Manion and T.A.C. Stock: *Int. J. Fract. Mech.*, 1970, vol. 6, p. 106.
46. R.C. Glenn and W.C. Leslie: *Metall. Trans.*, 1971, vol. 2, p. 2945.
47. P.A. Thornton and F.A. Heiser: *Metall. Trans.*, 1971, vol. 2, p. 1496.
48. A.L. Wingrove: *Metall. Trans.*, 1973, vol. 4, p. 1829.
49. S.A. Manion and A.L. Wingrove: *J. Aust. Inst. Met.*, 1972, vol. 17, p. 158.
50. R.L. Woodward and R.L. Aghan: *Met. Forum.*, 1978, vol. 1, p. 180.
51. J.L. Derep: *Acta Metall.*, 1987, vol. 35, p. 1245.
52. M. Stelly, J. Legrand, and R. Dormeval: in *Shock-Wave and High-Strain-Rate Phenomena in Metals*, M.A. Meyers and L.E. Murr, eds., Plenum Press, New York, NY, 1981, p. 113.
53. R.W. Wright and R.C. Batra: *Proc. DYMAT 85, Int. Conf. on Mechanical and Physical Behavior of Materials under Dynamic Loading*, Paris, Sept. 1985, Les Editions de Physique, Les Ulis, C5–323.
54. J.H. Giovanola: *Mech. Mater.*, 1988, vol. 7, p. 73.
55. K. Cho, Y.C. Chi, and J. Duffy: *Metall. Trans. A*, 1990, vol. 21A, p. 1161.
56. S.C. Liao and J. Duffy: *J. Mech. Phys. Solids*, 1998, vol. 11, p. 2201.
57. J.H. Beatty, L.W. Meyer, M.A. Meyers, and S. Nemat-Nasser: *Shock-Wave and High-Strain-Rate Phenomena in Materials*, Marcel Dekker, New York, NY, 1992, pp. 645–56.
58. Y. Meunier R. Roux, and J. Moureaud: *Shock Wave and High-Strain-Rate Phenomena in Materials*, M. Dekker, New York, NY, 1992, pp. 637–44.
59. M.A. Meyers and C.L. Wittman: *Metall. Trans. A*, 1990, vol. 21A, p. 3153.
60. C.L. Wittman, M.A. Meyers, and H.-R. Pak: *Metall. Trans. A*, 1990, vol. 21A, p. 707.
61. Q. Xue, M.A. Meyers, and N.F. Nesterenko: *Acta Mater.*, 2002, vol. 50, p. 575.
62. Q. Xue, M.A. Meyers, and N.F. Nesterenko: *Mater. Sci. Eng.*, 2004, vol. A384, p. 35.
63. M.A. Meyers, Y.B. Xu, Q. Xue, M.T. Perez-Prado, and T.R. McNelley: *Acta Mater.*, 2003, vol. 51, p. 1307.
64. R.C. Batra and G.M. Zhang: *J. Comput. Phys.*, 2004, vol. 201, p. 172.
65. D.G. Lee, Y.G. Kim, D.H. Nam, S.M. Hur, and S. Lee: *Mater. Sci. Eng.*, 2005, vol. A391, p. 221.
66. Q. Xue and G.T. Gray: *Metall. Mater. Trans. A*, 2006, vol. 37A, p. 2447.
67. E. Cerreta, Q. Xue, and G.T. Gray: *Acta Mater.*, 2007, vol. 55, pp. 691–704.
68. B.K. Kad, J.-M. Gebert, M.T. Perez-Prado, M.E. Kassner, and M.A. Meyers: *Acta Mater.*, 2006, vol. 54, pp. 4111–27.
69. Y.L. Bai, J. Bai, H.L. Li, F.J. Ke, and M.F. Xia: *Int. J. Impact Eng*, 2000, vol. 24, pp. 685–701.
70. R.W. Chen and K.S. Vecchio: *J. Phys. IV*, 1994, vol. C8, pp. 459–64.
71. L. Magness: *Mech. Mater.*, 1994, vol. 17, pp. 147–54.
72. G. Subhash, B.J. Pletka, and G. Ravichandran: *Metall. Mater. Trans. A*, 1997, vol. 28A, p. 1470.
73. M.A. Meyers, Y.J. Chen, and F.D.S. Marquis: *Metall. Trans.*, 1995, vol. 26A, p. 2493.
74. A. Hines and K.S. Vecchio: *Acta Mater.*, 1997, vol. 45 (2), pp. 635–49.
75. S. Nemat-Nasser and J.B. Isaacs: *Acta Mater.*, 1997, vol. 45, pp. 907–19.
76. L.W. Meyer and S. Manwaring: *Metallurgical Application of Shock-Wave and High-Strain-Rate Phenomena*, Marcel Dekker, New York, NY, 1986, p. 657.
77. Y.B. Xu, W.L. Zhong, Y.J. Chen, L.T. Shen, Q. Liu, Y.L. Bai, and M.A. Meyers: *Mater. Sci. Eng.*, 2001, vol. A299, p. 287.
78. C.A. Bronkhorst, E.K. Cerreta, Q. Xue, P.J. Maudlin, T.A. Mason, and G.T. Gray III: *Int. J. Plast.*, 2006, vol. 22, pp. 1304–35.
79. Q. Xue, G.T. Gray III, B.L. Henrie, S.A. Maloy, and S.R. Chen: *Metall. Mater. Trans. A*, 2005, vol. 36A, pp. 1471–86.
80. V.F. Nesterenko and M.P. Bondar: *DYMAT J.*, 1994, vol. 1, p. 243.
81. V.F. Nesterenko, M.A. Meyers, and T.W. Wright: *Acta Mater.*, 1998, vol. 46, p. 327.
82. Q. Xue, V.F. Nesterenko, and M.A. Meyers: *Int. J. Impact Eng.*, 2003, vol. 28, pp. 257–80.
83. Q. Xue, L.T. Shen, and Y.L. Bai: *Rev. Sci. Instrum.*, 1995, vol. 66, p. 5298.
84. Y.B. Xu and M.A. Meyers: *J. Mater. Sci. Technol.*, 2006, vol. 22, p. 737.
85. A. Molinari and R.J. Clifton: *C.R. Acad. Sci.*, 1983, vol. 296, p. 1.

86. D.E. Grady and M.E. Kipp: *J. Mech. Phys. Solids*, 1987, vol. 35, p. 95.
87. S. Kuriyama and M.A. Meyers: *Metall. Trans. A*, 1986, vol. 17A, p. 443.
88. T.W. Wright and H. Ockendon: *Int. J. Plast.*, 1996, vol. 12, p. 927.
89. A. Molinari: *J. Mech. Phys. Solids*, 1997, vol. 45, p. 1551.
90. R.J. Clifton, J. Duffy, K.A. Hartley, and T.G. Shawki: *Scripta Metall.*, 1984, vol. 18, p. 443.
91. Y.L. Bai, C. Cheng, and S.B. Yu: *Acta Mech. Sinica.*, 1986, vol. 2, p. 1.
92. T.W. Wright and R.C. Batra: *Adiabatic Shear Bands in Simple and Dipolar Plastic Materials*, Proc. IUTAM Symp. on Macro- and Micro-Mechanics of High Velocity Deformation and Fracture, K. Kawata J. Shioiri, eds., Springer, Berlin, 1987, p. 189.
93. T.G. Shawki and R.J. Clifton: *Mech. Mater.*, 1989, vol. 8, p. 13.
94. D. Xing, Y.L. Bai, C.M. Chen, and X.L. Huang: *J. Mech. Phys. Solids*, 1991, vol. 39, p. 1017.
95. S.C. Liao and J. Duffy: *J. Mech. Phys. Solids*, 1998, vol. 46, p. 2201.
96. M.E. Backman, S.A. Finnegan, J.C. Shulz, and J.K. Pringle: in *Metallurgical Applications of Shock-Wave and High-Strain-Rate Phenomena*, L.E. Murr, K.P. Staudhammer and M.A. Meyers, eds., Marcel Dekker, New York, NY, 1986, p. 675.
97. Y.L. Bai: in *Mech. Proc. Materials at High Rates of Strain*, J. Harding, ed., JOP Publishing, Bristol, 1989, p. 99.
98. B. Dodd and Y.L. Bai: *Ductile Fracture and Ductility with Application to Metalworking*, Academic Press, London, 1987.
99. L. Anand, O. Dillon, T.A. Place, and B.F. Von Turkovich: *Int. J. Plast.*, 1990, vol. 6 (2).
100. L.S. Costin, E.E. Crisman, R.H. Hartley, and J. Duffy: *Proc. 2nd Conf. on Mechanical Properties at High Rates of Starin*, J. Harding, ed., Institute of Physics, London, 1979, p. 90.
101. K.A. Hartley, J. Duffy, and R.H. Hawley: *J. Mech. Phys. Solids*, 1987, vol. 35, p. 283.
102. A. Marchand and J. Duffy: *J. Mech. Phys. Solids*, 1988, vol. 36, p. 59.
103. J.H. Giovanola: *Mech. Mater.*, 1988, vol. 7, p. 59.
104. R. Dormeval: in *Materials at High Strain Rates*, T.Z. Blazynski, ed., Elsevier Applied Science, New York, NY, 1987, p. 71.
105. Y.L. Bai, C.M. Cheng, and Y.S. Ding: *Res. Mech.*, 1987, vol. 22, p. 313.
106. G..B. Olson, J.F. Mescall, and M. Azrin: in *Shock-Wave and High-Strain-Rate Phenomena*, L.E. Murr and M.A. Meyers, eds., Plenum Press, New York, NY, 1981, p. 221.
107. M.R. Staker: *Acta Metall.*, 1981, vol. 29, p. 633.
108. S.L. Semiatin and G.D. Lahoti: in *Material Behavior under High Stress and Ultra-High Loading Rates*, J. Mescall and V. Weiss, eds., Plenum Press, New York, NY, 1983, p. 119.
109. F.H. Wu and L.B. Freund: *J. Mech. Phys. Solids*, 1987, vol. 32, p. 185.
110. M.E. Backman and S.A. Finnegan: in *Metallurgical Effects at High Strain Rates*, R.W. Rohde, B.M. Butcher, J.R. Holland, and C.H. Karnes, eds., Plenum Press, New York, NY, 1973, p. 531.
111. A.J. Bedford, A.L. Wingrove, and K.R.L. Thompson: *J. Aust. Inst. Met.*, 1974, vol. 19, p. 61.
112. S.P. Timothy and J.M. Hutchings: *Proc. 3rd Int. Conf. on Mechanical Properties at High Rates of Strain*, J. Harding, ed., Institute of Physics, Bristol, 1984, p. 397.
113. A. Molinari: in *Nonlinear Phenomena in Material Sciences Solid State Phenomena*, G. Martin and L.P. Kubin, eds., Trans Tech Publications, Aedermannsdorf, Switzerland, 1988, vol. 3–4, pp. 447–68.
114. T.W. Wright: *The Physics and Mathematics of Shear Bands*, Cambridge University Press, UK, 2002.
115. A.K. Zurek: *Metall. Mater. Trans. A*, 1994, vol. 25A, p. 2483.
116. Y.L. Bai: *J. Mech. Phys. Solids*, 1982, vol. 30, p. 195.
117. Y.B. Xu, L. Liu, J.Q. Yu, L.T. Shen, and Y.L. Bai: *Mater. Sci. Technol.*, 2000, vol. 16, p. 609.
118. Q. Li, Y.B. Xu, and M.N. Bassim: *J. Mater. Process. Technol.*, 2004, vol. 155, p. 1889.
119. H.C. Rogers and C.V. Shastry: in *Shock-Wave and High-Strain-Rate Phenomena in Metals*, M.A. Meyers and L.E. Murr, eds., Plenum Press, New York, NY, 1981, p. 285.
120. E.M. Trent: *JISI*, 1941, vol. 143, p. 401.
121. W.E. Carrington and M.L.V. Gayler: *Proc. R. Soc. London*, 1948, vol. A194, p. 323.
122. J.H. Andrews, H. Lee, and L. Bourne: *JISI*, 1950, vol. 165, p. 374.
123. N.C. Welsh: *J. Appl. Phys.*, 1957, vol. 28, p. 960.
124. H.O. McIntire and G.K. Manning: *Met. Prog.*, 1958, Nov, p. 94.
125. E. Rabinowicz: *Friction and Wear of Materials*, Wiley, New York, NY, 1965, p. 86.
126. D. Scott, B. Loy, and G.H. Mills: *Inst. Mech. Eng. Proc.*, 1966–67, vol. 181, p. 30.
127. K. Nakajima and Y. Mizutani: *Wear*, 1969, vol. 13, p. 283.
128. J.V. Craig and T.A.C. Stock: *J. Aust. Inst. Met.*, 1970, vol. 15, p. 1.
129. T.A.C. Stock and A.L. Wingrove: *J. Mech. Eng. Sci.*, 1971, vol. 13, p. 110.
130. A.L. Wingrove: *J. Aust. Inst. Met.*, 1971, vol. 16, p. 67.
131. S.J. Manganello and K.H. Abbott: *J. Mater.*, 1972, vol. 7, p. 231.
132. T.S. Eyre and A. Baxter: *Metall. Mater.*, 1972, vol. 6, p. 435.
133. A.L. Wingrove and G. Wulf: *J. Aust. Inst. Met.*, 1973, vol. 18, p. 167.
134. S.P. Timothy and I.M. Hutchings: *Acta Metall.*, 1985, vol. 33, p. 667.
135. R.E. Winter: *Philos. Mag.*, 1975, vol. 31, p. 765.
136. M. Zhou, A.J. Rosakis, and G. Ravichandran: *J. Mech. Phys. Solids*, 1996, vol. 44, p. 981.
137. M. Zhou, G. Ravichandran, and A.J. Rosakis: *J. Mech. Phys. Solids*, 1996, vol. 44, p. 1007.
138. Y.B. Xu and M.A. Meyers: *J. Mater. Sci. Technol.*, 2003, vol. 19, p. 385.
139. J.L. Derep: *Acta Metall.*, 1987, vol. 35, p. 1245.
140. E.E. Crisman, J. Duffy, and Y.C. Chi: *Proc. ASME Symp. on Exp. Techn. in Micromechanics*, W.N. Sharpe, Jr., ed., AIME, New York, NY, 1989, p. 163.
141. P.R. Guduru, A.J. Rosakis, and G. Ravichandran: *Mech. Mater.*, 2001, vol. 33, p. 371.
142. J. Duffy and Y.C. Chi: *Mater. Sci. Eng.*, 1992, vol. A157, p. 195.
143. C.O. Mgbokwere, S.R. Nutt, and J. Duffy: *Mech. Mater.*, 1994, vol. 17, p. 97.
144. S.P. Timothy: *Acta Mater.*, 1987, vol. 35, p. 301.
145. C.Z. Duan: Doctoral Thesis, Dalian University of Technology, Dalian, China, 2004.
146. Y.B. Xu, J.H. Zhang, and M.A. Meyers: *Dynamic Recrystallization in the Shear Bands of Fe-Cr-Ni Monocrystal: Electron Backscatter Diffraction Characterization*, unpublished research.
147. K.P. Staudhammer, C.E. Frantz, S.S. Hecker, and L.E. Murr: *Shock-Wave and High-Strain-Rate Phenomena in Metals and Alloys*, Addison Dekker, New York, NY, 1981, p. 91.
148. L.E. Murr and M.F. Ross: *Philos. Mag.*, 1968, vol. 18, p. 281.
149. H.J. Kestenbach and M.A. Meyers: *Metall. Trans. A*, 1976, vol. 7A, p. 1943.
150. G.B. Olson and M. Cohen: *Metall. Trans. A*, 1976, vol. 7A, p. 1897.
151. M.A. Meyers, B.Y. Cao, V.F. Nesterenko, D. Benson, and Y.B. Xu: *Metall. Mater. Trans. A*, 2004, vol. 35A, p. 2575.
152. M.G. Mendiratta, A.K. Chakrabarti, and J.A. Roberson: *Metall. Trans.*, 1974, vol. 5, p. 1949.
153. G. Lutjering and S. Weissmann: *Acta Mater.*, 1970, vol. 18, p. 785.
154. D. Li and X. Wan: *Acta Metall. Sinica*, 1984, vol. 20, p. 375.
155. C.E. Shamblen: *Metall. Trans.*, 1972, vol. 2, p. 277.
156. L.S. Costin, E.E. Crisman, R.H. Hawley, and J. Duffy: *2nd Conf. on the Mechanical Properties of Materials at High Rates of Strain*, J. Harding, ed., The Institute of Physics; J. Eng. Mater. Technol., 1979, vol. 101, p. 258.
157. T. Shawki, R.J. Clifton, and G. Majda: Brown University Report ARO DAAG29-81-K-012/3, Brown University, Providence, RI, 1983.
158. K.A. Hartley, J. Duffy, and R.H. Hawley: *J. Mech. Phys. Solids*, 1987, vol. 35, p. 283.
159. Y.B. Xu, X. Wang, Z.G. Wang, L.M. Luo, and Y.L. Bai: *Scripta Mater.*, 1990, vol. 24, p. 571.
160. Y.B. Xu, Y.L. Bai L.T. Shen, and Q. Xue: in *Metallurgical and Materials Application of Shock-Waves and High-Strain-Rate Phenomena*, L.E. Murr, K.P. Staudhammer, and M.A. Meyers, eds., Elsevier Science, Amsterdam, 1995, p. 389.

161. Y.B. Xu, Z.G. Wang, X.L. Huang, D. Xing, and Y.L. Bai: *Mater. Sci. Eng.*, 1989, vol. A114, p. 81.
162. Y.B. Xu, Z. Ling, X. Wu, and Y.L. Bai: *J. Mater. Sci. Technol.*, 2002, vol. 18, p. 504.
163. S. Lee, K.M. Cho, K.C. Kim, and W.B. Choi: *Metall. Trans. A*, 1993, vol. 24A, p. 895.
164. K. Cho, S. Lee, Y.W. Chang, and J. Duffy: *Metall.Trans. A*, 1991, vol. 22A, p. 367.
165. Z. Ling: *J. Compos. Mater.*, 2000, vol. 34, p. 101.
166. Z. Ling, L. Luo, and B. Dodd: *J. Phys. III*, vol. 4, 1994, p. 453.
167. M. Zhou: *Int. J. Plast.*, 1998, vol. 14, p. 733.
168. L.H. Dai, Z. Ling, and Y.L. Bai: *Scripta Mater.*, 1999, vol. 41, p. 2452.
169. C.C. Koch, O.B. Cavin, C.G. McKamey, and J.O. Scarbrough: *Appl. Phys. Lett.*, 1983, vol. 43, p. 1017.
170. R.B. Schultz and C.C. Koch: *Appl. Phys. Lett.*, 1986, vol. 49, p. 146.
171. E. Hellstern and L. Schultz: *Mater. Sci. Eng.*, 1988, vol. 97, p. 39.
172. A.W. Weeber and H. Bakker: *Physica B*, 1998, vol. 153, p. 93.
173. A.Y. Yermakov, Y.Y. Yurchikov, and V.A. Barinov: *Phys. Met. Metall.*, 1981, vol. 52, p. 50.
174. C. Politis and W.L. Johnson: *J. Appl. Phys.*, 1986, vol. 60, p. 1147.
175. E. Gaffet and M. Harmelin: *J. Less Common Met.*, 1990, vol. 157, p. 201.
176. L. Schultz: *J. Less Common Met.*, 1988, vol. 145, p. 233.
177. C.M. Glass, G.M. Moss, and S.K. Golaski: in *Response of Metals to High Velocity Deformation*, P. Shewmon and V.F. Zackay, eds., AIME, New York, NY, 1961, p. 115.
178. C. Mataya, M.J. Carr, and G. Krauss: *Metall. Trans. A*, 1982, vol. 13A, p. 1263.
179. Q. Li, Y.B. Xu, Z.H. Lai, Y.L. Bai, and L.T. Shen: *J. Mater. Sci. Technol.*, 1999, vol. 15, p. 435.
180. J.F.C. Lins, H.R.Z. Sandim, H.-J. Kestenbach, D. Raabe, and K.S. Vecchio: *Mater. Sci. Eng. A*, 2007, vol. 457, pp. 205–11.
181. U. Andrade, M.A. Meyers, K.S. Vecchio, and A.H. Chokshi: *Acta Metall.*, 1994, vol. 42, p. 3183.
182. J.A. Hines and K.S. Vecchio: in *Metallurgical and Materials Applications of Shock-Wave and High-Strain-Rate Phenomena*, L.E. Murr, K. Staudhammer, and M.A. Meyers, eds., Elsevier Science, Amsterdam, 1995, p. 421.
183. L.E. Murr, C.-S. Niou, S. Pappu, J.M. Rivas, and S.A. Quinones: *Phys. Status Solidi (a)*, 1995, vol. 149, p. 253.
184. J.A. Hines, K.S. Vecchio, and S. Ahzi: *Metall. Mater. Trans. A*, 1998, vol. A29, p. 191.
185. S. Pappu, C.S. Niou, C. Kennedy, L.E. Murr, L. DuPlessis, and M.A. Meyers: in *Metallurgical and Materials Applications of Shock-Wave and High-Strain-Rate Phenomena*,. L.E. Murr, K. Staudhammer, and M.A. Meyers, eds., Elsevier Science, Amsterdam, 1995, p. 495.
186. L.E. Murr, C.S. Niou, and C. Feng: *Scripta Metall.*, 1994, vol. 34, p. 297.
187. V.F. Nesterenko, M.A. Meyers, J.C. LaSalvia, M.P. Bondar, Y.J. Chen, and Y.L. Lukyanov: *Mater. Sci. Eng.*, 1997, vol. A229, p. 23.
188. M.A. Meyers, V.F. Nesterenko, J.C. LaSalvia, Y.B. Xu, and Q. Xue: *J. Phys. IV*, 2000, vol. 19, p. 9.
189. Q. Li, Y.B. Xu, Z.H. Lai, L.T. Shen, and Y.L. Bai: *Mater. Sci. Eng.*, 2000, vol. A276, p. 250.
190. M.A. Meyers, J.C. LaSalvia, V.F. Nesterenko, Y.J. Chen, and B.K. Kad: in *Recrystallization and Related Phenomena, Rex* '96, T.R. McNelley, ed., Monterey, CA, 1997, pp. 27–29.
191. K. Cho, S. Lee, S.R. Nutt, and J. Duffy: *Acta Mater.*, 1993, vol. 41, p. 923.
192. B. Derby: *Acta Metall. Mater.*, 1991, vol. 39, p. 955.
193. J. Hynes, K.S. Vecchio, and S. Ahzi: *Metall. Mater. Trans. A*, 1998, vol. 29A, p. 191.
194. J.D. Campbell, J.A. Simmons, and J.E. Dorn: *J. Appl. Mech.*, 1961, vol. 28, p. 447.
195. H.J. Frost and M.F. Ashby: *Deformation Mechanism Maps*, Pergamon, Oxford, United Kingdom, 1982, p. 26.
196. Q. Li: Post-D Research Report, Institute of Metal Research, Chinese Academy of Sciences, Shenyang, China, 1999, pp. 47–48.
197. J.G.. Sevillano, P. van Houtte, and E. Aernoudt: *Prog. Mater Sci.*, 1981, vol. 25, pp. 69–199.
198. D.A. Hughes and N. Hansen: *Acta Mater.*, 1997, vol. 45, p. 3871.
199. D.A. Hughes, R.A. Lebensohn, H.R. Wenk, and A. Kumar: *Proc. R. Soc. London, Ser. A*, 2000, vol. 456, p. 921.
200. F.J. Humphreys and M. Hatherly: *Recrystallization and Related Annealing Phenomena*, Pergamon, Oxford, United Kingdom, 1995.
201. M.E. Kassner and M.T. Peres Prado: *Fundamentals of Creep in Metals and Alloys*, Elsevier, New York, 2004.
202. B. Dodd and Y.L. Bai: *Mater. Sci. Eng.*, 1989, vol. 5, p. 557.
203. P.G. Shewmon: *Diffusion in Solids*, 2nd ed., TMS-AIME, Warrendale, PA, 1989, p. 3.
204. A.W. Weeber and H. Bakker: *Physica B*, 1998, vol. 153, p. 95.
205. M.F. Ashby and R.A. Verrall: *Acta Metall.*, 1973, vol. 21, p. 149.
206. L.E. Murr, E.A. Trillo, S. Pappu, and C. Kennedy: *J. Mater. Sci.*, 2002, vol. 37, p. 3337.
207. L.E. Murr: in *Materials at High Strain Rates*, T.E. Blazynski, ed., Elsevier Applied Science, New York, NY, 1987, p. 1.
208. M.A. Meyers, V.F. Nesterenko, J.C. LaSalvia, and Q. Xue: *Mater. Sci. Eng.*, 2001, vol. A317, p. 204.
209. L.E. Murr: *Interfacial Phenomena in Metals and Alloys*, Addison-Wesley, New York, NY, 1975.
210. R. Dormeval: in *Shock-Wave and High Strain Rates in Metals*, M.A. Meyers and L.E. Murr, eds., Plenum Press, New York, NY, 1981, p. 49.
211. A.J. Bedford, A.L. Wingrove, and K.R.L. Rhompson: *J. Aust. Inst. Met.*, 1974, vol. 19, p. 61.
212. S. Lee, K.-M. Cho, C.S. Lee, and W.Y. Choo: *Metall. Mater. Trans. A*, 1993, vol. 24A, p. 2217.
213. M.A. Meyers, U.R. Andrade, and A.H. Chokshi: *Metall. Mater. Trans. A*, 1995, vol. 26A, p. 2881.
214. D.G. Brandon: in *Materials at High Strain Rates*, T.E. Blazynski, ed., Elsevier Applied Science, New York, NY, 1987, p. 187.
215. J.Q. Yu: Master's Thesis, Institute of Metal Research, Chinese Academy of Sciences, Shenyang, China, 1999.
216. Z.F. Zhang and Y.B. Xu: *Acta Mater. Sinica*, 1986, vol. 21, p. 384.
217. Q. Xue and G.T. Gray: *Metall. Mater. Trans. A*, 2006, vol. 37A, p. 2447.
218. M. Zhou, A.J. Rosakis, and G. Ravichandran: *J. Mech. Phys. Solids*, 1996, vol. 44, p. 981.
219. S. Mercier and A. Molinari: *J. Mech. Phys. Solids*, 1998, vol. 46, p. 1463.
220. E. Grady: *Mech. Mater.*, 1994, vol. 17, p. 289.
221. A.H. Chokshi and M.A. Meyers: *Scripta Metall.*, 1990, vol. 24, pp. 605–10.
222. A. Mishra, B.K. Kad, F. Gregori, and M.A. Meyers: *Acta Mater.*, 2007, vol. 55, p. 13.
223. H.S. Kim, D.H. Joo, M.H. Kim, S.K. Hwang, S.I. Kwun, and S.W. Chae: *Mater. Sci. Technol.*, 2003, vol. 19, p. 403.
224. S. Walley: *Metall. Mater. Trans. A*, 2007, vol. 38, pp. 2629–54.
225. R.D. Conner, Y. Li, W.D. Nix, and W.L. Johnson: *Acta Mater.*, 2004, vol. 52, pp. 2429–34.
226. U.F. Kocks and H. Mecking: *Prog. Mater. Sci.*, 2003, vol. 48, pp. 171–273.
227. A. Molinari and G. Ravichandran: *Mech. Matls.*, 2005, vol. 37, pp. 737–52.
228. A. Rosakis and G. Ravichandran: *Int. J. Sol. Struct.*, 2000, vol. 37, pp. 331–3348.
229. A. Molinari, E.A. Olevsky and M.A. Meyers: *unpublished results*, 2007.
230. W.D. Nix: *personal communication*, 2006.
231. L.W. Meyer: *personal communication*, 2007.
232. F. Spaepen: *Acta Metal.*, 1977, vol. 25, p. 407.
233. L.F. Liu, L.H. Dai, Y.L. Bai, and B.C. Wei: *J. Non-Cryst. Solids*, 2005, vol. 351, pp. 3259–70.
234. L.H. Dai, M. Yan, L.F. Liu, and Y.L. Bai: *Appl. Phys. Lett.,* 2005, vol. 87, pp. 141916-1–4.